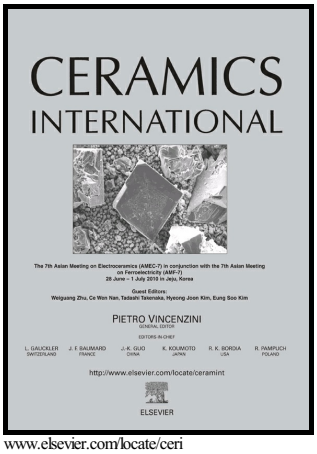

www.elsevier.com/locate/ceri

Karrooite green pigments doped with Co and Zn: synthesis, color properties and stability in ceramic glazes

M. Llusar, T. Bermejo, J.E. Primo, C. Gargori, V. Esteve, G. Monrós

PII: S0272-8842(17)30670-3
DOI: http://dx.doi.org/10.1016/j.ceramint.2017.04.062
Reference: CERI15042

To appear in: *Ceramics International*

Cite this article as: M. Llusar, T. Bermejo, J.E. Primo, C. Gargori, V. Esteve and G. Monrós, Karrooite green pigments doped with Co and Zn: synthesis, colo properties and stability in ceramic glazes, *Ceramics Internationa* http://dx.doi.org/10.1016/j.ceramint.2017.04.062

Karrooite green pigments doped with Co and Zn: synthesis, color properties and stability in ceramic glazes

M. Llusar*, T. Bermejo, J.E. Primo, C. Gargori, V. Esteve, G. Monrós

Departamento de Química Inorgánica y Orgánica, Universitat Jaume I, 12071, Castellón, Spain.

* **Corresponding author.** Departament de Química Inorgànica y Orgànica, Universitat Jaume I, Edifici Científico-Tècnic, Av. Sos Baynat s/n, 12071, Castelló, Spain, Tfn number: +34 964 728244, Fax number: +34 964 728214, E-mail: mllusar@uji.es

Abstract

The solid-state synthesis and stabilization of Co doped ($Mg_{1-x}Co_xTi_2O_5$), Zn doped ($Mg_{1-x}Zn_xTi_2O_5$) and Co- and Zn-codoped karrooite solid solutions ($Mg_{0.8-x}Zn_{0.2}Co_xTi_2O_5$ and $(Mg_{0.5}Zn_{0.5})_{1-x}Co_xTi_2O_5$) were investigated. In addition, the optical spectra, color properties and technological performance of (Co,Zn)-karrooite compositions as new green ceramic pigments were also analyzed. XRD characterization revealed for the first time the high solid solubility of Zn^{2+} in $MgTi_2O_5$ karrooite at 1200 ºC (between 60 and 80 mol% per Mg or karrooite formula unit). In contrast, the reactivity and stabilization of karrooite phase decreased in the case of Co^{2+} doping. Interestingly, codoping with Zn^{2+} ions at high molar ratios (Zn:Mg ratio equal to 1:1) enhanced the reactivity and enabled the stabilization of (Co,Zn)-$MgTi_2O_5$ karrooite solid solutions, even with high Co^{2+} loadings (20 mol% per karrooite formula unit). The (Co,Zn)-$MgTi_2O_5$ pigments exhibited yellowish-green colors associated to Co^{2+} ions allocated in octahedral M1 and M2 sites of karrooite lattice, and becoming more intense and less yellow the higher the Co content. However, Zn^{2+} codoping produced less saturated green colors with similar green but lower yellowish hues. The obtained pigments were not stable enough within the tested ceramic glazes, giving rise to turquoise colorations due to cobalt leaching and incorporation into tetrahedral sites of the glassy phase. The stability of Co-karrooite green

pigments was higher in a Ca- and Zn-enriched ceramic glaze (B) fired at a higher temperature (1050 ºC).

Keywords:

Color (C); TiO_2 (D); Transition metal oxides (D); Pseudobrookite pigments (E).

1. Introduction

Karrooite is the non-official name provided for synthetic magnesium-titanium pseudobrookite ($MgTi_2O_5$), which crystallizes in orthorhombic symmetry and *Cmcm* (63) space group [1]. In the last years, karrooite has been investigated as potential host lattice for the preparation of ceramic pigments. For instance, karrooite solid solutions doped with different transition metal chromophore ions ($Mg_{1-x}M_{2x}Ti_{2-x}O_5$, x = 0.02 and 0.05, M= Co^{2+}, Cr^{4+}, Fe^{3+}, Mn^{2+}/ Mn^{3+}, Ni^{2+} and V^{4+}) were prepared by the classical ceramic route from mixtures of oxide precursors (fired at 1300 ºC) and analyzed as alternative ceramic pigments [2]. The obtained colors were found stable in low-temperature (<1050 °C) ceramic glazes and glassy coatings, although they were rather unstable in highly opacified glazes containing large amounts of CaO and ZnO. In the case of Ni^{2+}-doping, the whole range of Ni:$MgTi_2O_5$ solid solutions ($Mg_{1-x}Ni_{2x}Ti_{2-x}O_5$) has been also recently investigated [3], giving rise to intense yellowish orange pigments with increased chromaticity and saturation the higher the Ni content (up to x=0.4-0.5).

In regard to Co^{2+}-doped karrooite pigments, Matteucci *et al.* on [2] investigated the effect of relatively low Co loadings (4 and 10 mol% with respect to karrooite). Interestingly, the obtained Co^{2+}-doped karrooite powders were green-colored, which is less common for Co^{2+}-based pigments. Indeed, the color of Co^{2+} pigments can range from blue, green to violet or pink depending on the host lattice and coordination environment, although pink is the usual color when cobalt is accommodated in octahedral sites, and much more intense or deep blue colors

are generally associated to cobalt in tetrahedral coordination [4–6]. Today a common source of green color for the ceramic industry is a mixture of Pr-zircon yellow and V-zircon blue pigments, since other alternative green pigments contain large amounts of toxic and pollutant elements such as Cr, Co or Ni ("green of Sèvres" based on Cr_2O_3; Uvarovite green garnet, $Ca_3Cr_2Si_3O_{12}$, with CPMA number 04-07-3 [7]; cobalt chromite green spinel, $CoCr_2O_4$, with CPMA number 13-30-3; cobalt titanate green spinel, Co_2TiO_4,with CPMA number 13-31-3; and nickel silicate green olivine, Ni_2SiO_4, with CPMA number 05-45-3). In this respect, the employment of allochromatic solid solutions doped with a low or minimized amount of Co (Ni or Cr) may be an interesting, less-pollutant and less-expensive alternative for green ceramic pigments [8–11], instead of idiochromatic (non-substituted) pigments of $CoCr_2O_4$, Co_2TiO_4 and Ni_2SiO_4.

With the above precedents, in the present investigation we scrutinized the formation by ceramic route of $MgTi_2O_5$-$CoTi_2O_5$ greenish solid solutions ($Mg_{1-x}Co_xTi_2O_5$) in a more extended compositional range (up to 40 mol% of Co per karrooite unit formula, due to the environmental concerns previously mentioned). $CoTi_2O_5$ crystallizes in the same pseudobrookite structure as $MgTi_2O_5$ karrooite, and it is also an entropy-stabilized phase [12–14]; it becomes more stable the higher the temperature, and below 1142 ºC it decomposes in a mixture of the more stable $CoTiO_3$ ilmenite and TiO_2 rutile phases [15–17]. Given the isomorphism between Co-Ti and Mg-Ti pseudobrookites as well as the quite similar effective ionic radii for Co^{2+} (74.5 pm) and Mg^{2+} (72 pm) ions in octahedral coordination [18], we could expect a whole range of solid solubility of Co ions in $MgTi_2O_5$ karrooite.

Moreover, we also investigated the effect of Zn^{2+} codoping on the stabilization of Co-doped karrooite solid solutions ($Mg_{1-x-y}Co_xZn_yTi_2O_5$), the color and optical properties of the resulting pigments, and its industrial performance either as ceramic pigments or dyes within ceramic glazes [19–23]. In spite of the existence of some precedent investigations analyzing the effect of Co- and Zn-codoping on related $MgTiO_3$ ilmenites (in order to improve its dielectric properties) [24,25], as far as we know there are not preliminary reports in the literature concerning Co- and

Zn-codoped $MgTi_2O_5$ karrooite. In addition, there is also no experimental evidence of the synthesis of $ZnTi_2O_5$ with a parent structure to $MgTi_2O_5$ and $CoTi_2O_5$ pseudobrookites. Indeed, although some $TiO_2{\cdot}xZnO$ compositions including $ZnTi_2O_5$ stoichiometry have been prepared as high frequency dielectric materials [26] or as photoactive $ZnTi_2O_5$ thin films for solar cells [27], the supposed crystallization of $ZnTi_2O_5$ was not demonstrated.

In this respect, different ternary compounds with interesting technological applications are already known as stable phases in the Zn-Ti-O ternary system [28–31], such as Zn_2TiO_4 inverse cubic spinel, $ZnTiO_3$ rhombohedral ilmenite and $Zn_2Ti_3O_8$ cubic defect spinel. Interestingly, other unreported or missing phases in this system have been very recently predicted to be borderline stable, such as $ZnTi_2O_4$ normal spinel, $ZnTi_2O_5$ pseudobrookite (chemically similar or equivalent to $MgTi_2O_5$ karrooite), and $ZnTi_5O_{10}$ in the high-symmetry Ti_3O_5 pseudobrookite structure [32]. As experimental evidence, the related $Zn_xTi_{3-x}O_5$ phase (with $x \approx 0.6$) was successfully synthesized in this recent study, adopting essentially the same structure as $ZnTi_5O_{10}$. This compound was found as much stable as the other unreported ternary Zn-Ti-O phases, highlighting the interest to perform further explorative investigations on these missing materials of the Zn-Ti-O system, including $ZnTi_2O_5$ pseudobrookite.

Accordingly, in addition to the use of Zn as codoping agent in Co-$MgTi_2O_5$ pigments, in this study we firstly investigated the $MgTi_2O_5$:$ZnTi_2O_5$ system to elucidate the solid solubility limit of Zn^{2+} ions in karrooite lattice. In the case of Co-karrooite pigments, the addition of Zn^{2+} as codoping agent or structure modifier could induce a considerable color change due to modification of Co^{2+} octahedral crystal field [33] and the covalent character of Co-O bonds [34] in karrooite lattice. On the other hand, the choice of Zn^{2+} ions could also serve to improve the stability of Co-karrooite compounds as true ceramic pigments within Zn-Ca-borosilicate ceramic glazes, as it has been recently found in other Zn-containing pigments such as Co-doped $Ca_2(Zn,Co)Si_2O_7$ hardystonite [35].

2. Materials and methods

2.1. Samples preparation (Ceramic route)

A set of four different $(Mg_{1-x-y}Co_xZn_y)Ti_2O_5$ karrooite-based solid solutions (series) were prepared by the conventional ceramic route, using $Mg_5(CO_3)_4(OH)_2.xH_2O$ (42% as Mg, Aldrich), Co_3O_4 (70% as Co, Panreac), ZnO (98%, Panreac) and TiO_2 (anatase, 99-100.5%, Panreac) as precursors. The location of the four series compositions on a ternary Mg-Zn-Co diagram is shown in *Figure 1*. First of all, a whole series of Zn:karrooite solid solutions (***Kar-Zn*** series: $\boldsymbol{Mg_{1-x}Zn_xTi_2O_5}$, with x = 0, 0.1, 0.2, 0.4, 0.5, 0.6, 0.8 and 1.0) was prepared for the previous investigation on the $MgTi_2O_5$–$ZnTi_2O_5$ system. In regard to Co-doped samples, the ***Kar-Co*** series ($\boldsymbol{Mg_{1-x}Co_xTi_2O_5}$; x = 0.05, 0.1, 0.2 and 0.4) corresponds to Zn-free Co-karrooite compositions ($MgTi_2O_5$–$CoTi_2O_5$ system). Then, the ***Kar-CoZnL*** series ($\boldsymbol{Mg_{0.8-x}Zn_{0.2}Co_xTi_2O_5}$, with x = 0.05, 0.1 and 0.2) contains a relatively low and fixed amount of Zn (0.2 mol) per MTi_2O_5 karrooite formula unit, with Co only replacing Mg ions and having a variable Mg:Zn ratio. Finally, the ***Kar-CoZnH*** series ($\boldsymbol{(Mg_{0.5}Zn_{0.5})_{1-x}\,Co_xTi_2O_5}$, with x = 0.05, 0.1 and 0.2) was prepared with a considerably higher Zn doping level (0.4-0.475 mol of Zn^{2+} per karrooite formula unit), and using this time a fixed Mg:Zn ratio equal to 1:1 (note that in this series Co ions are equally replacing both Mg and Zn ions).

In a typical sample preparation, the corresponding stoichiometric mixture of precursors was homogenized in planetary mills (20 min) using acetone as dispersant. The dried powders were then directly calcined in an electrical furnace up to 1200 ºC with heating rate of 5ºC/min, a soaking time of 3 hours and with free cooling to room temperature. *Kar-Zn* samples were also subsequently fired at 1400 ºC (after due homogenization and micronization of previously fired compositions). After the firing treatment, all the fired powders were homogenized and micronized (mortar and pestle) and sieved below 63 μm before further characterization (section 2.2).

2.2. Samples characterization

Crystal chemical characterization of karrooite-based $(Mg,Zn,Co)Ti_2O_5$ calcined samples was performed by X-ray powder diffraction (XRD) in a D4 Endeavor (Bruker-AXS) powder

diffractometer with Cu-K_α radiation (from 10 to 70º 2θ, with steps of 0.05º 2θ and a counting time of 2s per step). The diffractometer was equipped with a graphite secondary monochromator to eliminate K_β and fluorescence signals. The cell parameters were also determined by indexing and least-squares refinement of XRD patterns of selected powder compositions mixed (50 wt%) with Al_2O_3 corundum as internal standard and measured under slower conditions (steps of 0.02º 2θ and a counting time of 4 s per step), using the POWCAL and LSQC programs (Department of Chemistry, University of Aberdeen, UK).

On the other hand, the microstructure and morphology of (Mg,Zn,Co)Ti_2O_5 fired samples was examined by scanning electron microscopy (SEM) with a JEOL 7001F electron microscope (following conventional preparation and imaging techniques). The chemical composition and homogeneity of the samples was determined by semi-quantitative elemental analysis with an EDX analyzer (supplied by Oxford University) attached to the microscope.

In order to analyze the stability and optical or coloring properties (pigmenting performance) of karrooite-based (Mg,Zn,Co)Ti_2O_5 solid solutions within conventional low-temperature ceramic glazes, the fired powders were 5 wt-% enameled within three different commercial transparent glazes (of relatively low firing temperature) onto conventional ceramic biscuits: glaze A of the SiO_2-Al_2O_3- K_2O -CaO-ZnO system (low Ca and Zn content, and free of Pb), glace B of the SiO_2-CaO-ZnO system (high Ca and Zn content, and free of Pb), and glaze C of the SiO_2-Al_2O_3-PbO-CaO-Na_2O-K_2O system (low Ca content, free of Zn but Pb-containing). Enameled samples were fired following fast-firing schedules (52 min of duration from cool to cool at a maximum temperature of 980, 1050 or 980ºC for glazes A, B and C respectively). The optical properties of fired powders and glazed samples were then analyzed by diffuse reflectance spectroscopy (UV-vis-NIR) performed with a Jasco V670 spectrophotometer. The color parameters (*L*a*b**) were also measured following the *CIE-L*a*b** colorimetric method recommended by the CIE (Commission Internationale de l'Eclairage) [36], using an 8/d geometry (diffused illumination of 8º), with the observer at 10º and a standard lighting D65. On

this method, L^* is the lightness axis (black (0) → white (100)), a^* is the green (-)→ red (+) axis, and b^* is the blue (-) → yellow (+) axis.

3. Results and discussion

3.1. Solid solubility of Zn in $MgTi_2O_5$ ($Mg_{1-x}Zn_xTi_2O_5$ solid solutions)

A whole set of Zn-karrooite solid solutions (***Kar-Zn***, $Mg_{1-x}Zn_xTi_2O_5$) was first prepared in order to elucidate the solid solubility limit of Zn^{2+} ions in karrooite. *Figure 2a* shows the evolution of crystalline phases with Zn content (x) in $Mg_{1-x}Zn_xTi_2O_5$ solid solutions fired at 1200 ºC. The $(Mg,Zn)Ti_2O_5$ pseudobrookite structure (karrooite; PDF file number 035-0796) was successfully stabilized as single phase up to x = 0.6 (60 mol% of Zn doping per karrooite), while $MgTiO_3$ ilmenite (PDF file number 006-0494) and TiO_2 rutile (PDF file number 021-1276) became the predominant phases for x = 0.8, still accompanied by a small amount of karrooite (XRD peaks of weak intensity); in the XRD pattern of x = 1.0 sample only this mixture of ilmenite and rutile phases was present.

Interestingly, a subsequent thermal treatment at a higher firing temperature (1400 ºC) did not succeed in increasing the range of solid solubility above x = 0.6, although reactivity increased considerably. As it may be observed in *Figure 2b*, at 1400 ºC the pseudobrookite $(Mg,Zn)Ti_2O_5$ solid solution formed again as almost single phase for compositions with $x \leq 0.6$, and it crystallized also as the major phase for composition x = 0.8, although being still accompanied by large amounts of ilmenite and rutile phases. In the case of end member composition (x = 1.0), the reacting mixture melted extensively and it could not be extracted from the crucible, nor analyzed. Accordingly, this investigation evidenced that the solid solubility limit of Zn^{2+} ions in $MgTi_2O_5$ karrooite under the employed firing conditions lies between 60 and 80 mol%. This fact enabled us to analyze the effect of Zn-codoping on Co-karrooite pigments employing not only relatively low amounts (20 mol% in *Kar-CoZnL* series) but also high Zn molar loadings (such as 40-47.5% in *Kar-CoZnH* series).

On the other hand, the XRD patterns of $Mg_{1-x}Zn_xTi_2O_5$ powders fired at 1400 ºC (up to x = 0.6, and mixed with Al_2O_3 corundum as internal standard) were also refined and indexed, according to orthorhombic symmetry and *Cmcm (63)* space group, in order to measure the cell parameters of karrooite lattice and analyze the effect of Zn doping. As it is well-known, it is not a simple task in doped karrooite compositions to separate the contributions on unit cell dimensions of both ionic radii variations and order-disorder effects; for instance, an increase of unit cell dimensions may arise not only from the introduction of a larger cation but also from an increase of cationic disorder (since this involves a higher ratio of the larger Mg ions on the smaller M2 octahedral sites of pseudobrookite lattice) [2,37,38]. The coexistence of both effects usually leads to irregular trends in the variation of unit cell dimensions in doped karrooite samples. In our case, *Figure 3* shows the evolution of cell parameters and cell volume with Zn content (*x*) in Zn-doped karrooite solid solutions ($Mg_{1-x}Zn_xTi_2O_5$). As it may be observed, Zn-doping produces an anisotropic variation of cell parameters, with a slight decrease of *a* parameter, an increase of *c* parameter and without any clear trend for *b* parameter. As a result, the unit cell volume decreases for the first doping stage (from $x = 0$ to 0.2), which could be explained by an increase of cationic ordering [12–14], while further Zn-doping ($x = 0.4$ and 0.6) causes a slight increase of unit cell volume, which would be in agreement with the slightly higher ionic radius of Zn^{2+} (74 pm) with respect to Mg^{2+} (72 pm) [18].

3.2. XRD characterization of (Co,Zn)-karrooite pigment powders.

The XRD patterns of (Co,Zn)-Karrooite solid solution pigments prepared by the ceramic route and fired at 1200 ºC are shown in *Figures 4a-4c*. These patterns confirmed the effective formation and relative stabilization of karrooite solid solutions, although with increasing quantities of residual $MgTiO_3$ ilmenite phase the higher the Co content in both *Kar-Co* ($Mg_{1-x}Co_xTi_2O_5$; without Zn codoping) and *Kar-CoZnL* series ($Mg_{0.8-x}Zn_{0.2}Co_xTi_2O_5$; 20 mol% of Zn). Therefore, the increase of Co-doping appears to decrease the reactivity or stabilization of karrooite in both series (free or with a low Zn doping level). However, and very remarkably, $(Mg,Zn,Co)Ti_2O_5$ pseudobrookite became stabilized as single crystalline phase in *Kar-CoZnH*

compositions (*Figure 4c*) having a considerably higher amount of Zn codoping ($(Mg_{0.5}Zn_{0.5})_{1-x}Co_xTi_2O_5$; 40-50 mol% of Zn). This result evidences a favourable effect of Zn codoping on the stabilization of Co-karrooite structure at higher molar loadings. This enhanced stabilization of (Co,Zn)-doped karrooite may arise either from an increase of configurational entropy (cationic disorder) with Zn codoping (above 20 mol%), or it could simply be due to kinetics reasons (increased solid-state reactivity), given the higher proportion of ZnO in raw mixtures, which would be therefore more reactive than Mg hydroxy-carbonate.

Similarly to *Kar-Zn* series, we measured also the unit cell parameters and volume of *Kar-Co* and *Kar-CoZnH* samples from XRD patterns, in order to evaluate both the effect of Co doping and of Zn codoping on karrooite unit cell. According to the representation shown in *Figure 5*, the variation of unit cell parameters with cobalt doping (*x*) in the case of *Kar-Co* series (free of Zn) was rather anisotropic and nearly insignificant. Nevertheless, the slight increase of unit cell volume with Co doping would be in agreement with the higher ionic radius of Co^{2+} (74.5 pm) with respect to Mg^{2+} (72 pm) ions in octahedral coordination [18]. Regarding to *Kar-CoZnH* series (containing a high level of Zn codoping), the increase of Co-doping produced again an irregular and almost negligible variation of unit cell dimensions. Finally, in a comparison of unit cell parameters of *Kar-Co* and *kar-CoZnH* compositions for a similar Co content (*x* value; up to $x = 0.2$), the overall cell volume was considerably higher in Zn-containing samples samples (*Kar-CoZnH* series), which is also in agreement with the larger ionic radius of Zn^{2+} ions (74 pm) replacing the smaller Mg^{2+} (72 pm).

3.3. Microstructure and morphology characterization (SEM/EDX)

SEM/EDX characterization was performed with selected compositions to gain further information about the morphology, homogeneity and semiquantitative composition of pigment powders at the microscale, analyzing the effect of both Co and Zn codoping. SEM images of representative pigment compositions fired at 1200 ºC (3 h) and belonging to *Kar-Co* ($x = 0$, 0.1, 0.2 and 0.4), *Kar-CoZnL* and *Kar-CoZnH* series ($x = 0.2$) are shown in *Figure 6*.

Regarding to *Kar-Co* ceramic pigments ($Mg_{1-x}Co_xTi_2O_5$), the fired powders contained rather compact and sintered particle aggregates (see *e.g.* Figure 6a, corresponding to non-sieved powder with $x = 0$) with variable sizes ranging from a few to *ca.* 50 μm. These aggregates consisted of smaller grain-like particles, with sizes between 1 and 4 μm and presenting more or less rounded morphologies, as it may be observed in SEM images of Figures 6b-6f. Noteworthy, the morphology or microstructure of pigment powders was very similar in all samples (irrespective of the amount of Co or Zn doping), apart from the slightly larger particle sizes observed for Zn-containing samples (compare *e.g.* SEM images of *Kar-Co*, *Kar-coZnL* and *Kar-CoZnH* samples with $x = 0.2$, in Figures 6c, 6e and 6f).

Semiquantitative EDX analyses were performed in different regions of samples aiming to determine the chemical composition and homogeneity of Co- and Zn-codoped Karrooite solid solutions. In general terms, the average sample compositions determined by EDX analyses (see Table 1) were not far from nominal formulations, although they showed a considerable deficiency of Mg and an excess of Co (lower Mg:Co ratio).

3.4. Color characterization of (Co,Zn)-karrooite pigment powders.

The effect of Co and Zn doping on the color intensity and chromaticity of the obtained (Co,Zn)-karrooite fired powders was also investigated, in order to evaluate their potential use as ceramic pigments. As it may be seen in Figure 7 (which also includes the measured *CIE-L*/a*/b** color parameters), all the obtained compositions exhibited a varied gamut of yellowish-green colors, with a considerable variation of color hue and intensity with Co and Zn doping. In order to facilitate the analysis of color variations in the different pigment series, Figure 8 shows the variation with Co content (x) of the greenish (negative a^* value) and yellowish (positive b^* value) color parameters (CIE system), related with the observed hue or chromaticity (Figure 8 above), and of the lightness L^* parameter (Figure 8 below) indirectly related to the color saturation or intensity (lower L^* values are normally associated with more saturated or intense colors). As it may be observed, the green hue was very similar in all samples (a^* between -9 and -11), with only a slight decrease with the increase of Co content (x)

in all series, and an almost negligible increase with Zn codoping when comparing (for the same Co content) the three series (*Kar-Co*, *Kar-CoZnL* and *Kar-CoZnH*).

Regarding to the yellowish hue (positive *b** value) the effect of Co and Zn doping was much more important: on the one hand, the increase of Zn codoping (for a given amount of Co) produced a progressive and considerable decrease of the yellow hue, the color of *Kar-CoZnH* pigments being less yellowish; on the other hand, the increase of Co doping also produced a considerable decrease of the yellow hue in both *Kar-Co* (from 16 to 11 up to $x = 0.2$; and a further decrease to 6 for $x = 0.4$) and *Kar-CoZnL* compositions (from 12 to 8 up to $x = 0.2$). In contrast, in *kar-CoZnH* pigments (with the highest level of Zn codoping) the measured yellow hue was much lower and showed only a very slight increase (from 5 to 6 up to $x = 0.2$). Finally, considering the color lightness (Figure 8, below), the increase of Co content resulted in the three series in an important and progressive increase of color intensity (lower lightness, *L**). On the contrary, the increase of Zn codoping for a constant amount of Co produced only a very slight increase of color saturation from *Kar-Co* to *Kar-CoZnL* series, while a further increase of Zn loading in the case of *Kar-CoZnH* series gave rise to lighter colors (higher L* values).

3.5. UV-VIS-NIR spectroscopy of (Co,Zn)-karrooite pigment powders.

The UV-vis-NIR absorption spectra (Kubelka Munk absorbance function, *K/S*) of Co-karrooite pigment powders (*Kar-Co*, $Mg_{1-x}Co_xTi_2O_5$) prepared by ceramic route and fired at 1200 ºC/3h are shown in Figure 9 (above). The absorption profiles of *Kar-Co* pigments presented similar features to those previously described by Matteucci *et al.* for cobalt-doped karrooite [2]. These spectra fit perfectly with the spectral features of Co^{2+} (a $3d^7$ ion) in octahedral coordination [33,39]. Noteworthy, the absorption bands are considerably red-shifted (resulting in green colors) with respect to those exhibited by octahedral-coordinated Co^{2+} ions in other pigment structures such as Co-olivines [40] or Ca,Co-pyroxenes [4], which develop the more usual violet or pink colorations.

As it may be observed, the spectra present the typical three spin-allowed transitions from Co^{2+} ground state ($^4T_{1g}$ (^4F)) to the different exited terms. The highest energy (and more intense)

band associated to ν_3 transition ($^4T_{1g}$ (^4F) $\rightarrow$ $^4T_{1g}$ (^4P)) is centered in the visible region at *ca.* 590 nm (yellow-orange region) leaving a deep reflection window around 500 nm which is responsible for the yellowish green colors of the pigments. Then, a much weaker or less intense band is observed extending from 700 to 900 nm, which is associated to the less-intense (two-electron) ν_2 transition ($^4T_{1g}$ (^4F) $\rightarrow$ $^4A_{2g}$ (^4F)). Finally, a very broad and double-peak band may be observed in the near-IR region extending from 1050 to 1650 nm, with the two peaks centered at around 1190 and 1430 nm, which is attributed to the lowest energy spin-allowed transition ν_1 ($^4T_{1g}$ (^4F) $\rightarrow$ $^4T_{2g}$ (^4F)). This clearly visible splitting of ν_1 transition could be attributed to the different local environments found by Co^{2+} ions at the non-equivalent M1 and M2 octahedral sites of karrooite, which causes the corresponding optical absorption bands to occur at different energies for both sites. However, this "splitting effect" was not so evident for ν_2 and ν_3 transitions. To this respect, a perfect deconvolution of the spectra (not shown) was not feasible without considering this doubling of all the spin-allowed transitions associated to both M1 and M2 sites (as it was also reported by Matteucci et al. [2]). Moreover, the small absorption contribution (shoulders) associated to other spin-forbidden transitions to ^2E_g (^2G), $^2T_{1g}$ + $^2T_{2g}$ (^2G) and $^2A_{1g}$ (^2G) excited terms (from lower to higher energy) must be also considered. The energy positions of these forbidden transitions are also indicated by arrows in Figure 9.

Remarkably, all the absorption bands occurred at very similar wavelength or energy values, irrespective of Co loading. This fact indicates that Co-O distances were not substantially changed with Co doping. Moreover, and as it was expected, the increase of Co doping was accompanied by an increase of the absorption band intensities or optical density (see Figures 7 and 8), which correlates perfectly with the observed increase in the saturation of the green color (lower L^* values). The increased color saturation (and darkness) of pigments induced by Co doping was also accompanied by a decrease of the yellow hue (b^* value), and this fact may be also correlated with the increased absorption in the yellow region (560-590 nm) observed in the optical spectra as the Co content increases.

The optical spectra of Zn-containing samples (*Kar-CoZnL* and *Kar-CoZnH* series) were also analyzed to investigate the effect of Zn codoping. In this respect, the important color change observed for Zn-codoped Co-karrooite solid solutions (with lighter and less yellowish green colors) must arise from changes in crystal field energy or intensity (exerted by O^{2-} ligands onto Co^{2+} ions) induced by the replacement of Mg^{2+} by the larger Zn^{2+} ions. Interestingly, the optical spectra of Zn-containing samples (*Kar-CoZnL* and *Kar-CoZnH* series) exhibited very similar features to those of Zn-free *Kar-Co* samples, especially in the case of samples with a low doping level (20 mol% of Zn). Indeed, Zn codoping did not produce any appreciable shift in the position of the bands attributable to significant variations of Co-O distances (and crystal field energy).

However, and as a remarkable fact, Co-karrooite samples with higher Zn codoping levels (40-47.5 mol% in *Kar-CoZnH* series) exhibited comparatively much broader and less intense absorption bands (lower optical density) associated with ν_3 *d-d* transition and with Co-O and Ti-O charge transfer transitions (see *e.g.* the effect of Zn codoping in the comparative spectra of Figure 9 below, for a given amount of Co doping, $x = 0.2$). As a result, the reflection window in the green region (around 500 nm) becomes considerably broader and less sharp, giving rise to lighter (higher L^*) green colors with a considerably lower yellowish hue (b^* value).

This important modification in the color and distinct absorption features for Co-karrooite samples at higher Zn-codoping levels could arise from a modification of the covalent/ionic character of cobalt-oxygen bonds in octahedral environments of karrooite lattice. In previous studies on related systems, this covalence modification has been attributed to the *competitive bond effect*, which implies that the covalence of one bond is correlated or affected by the strength of neighboring bonds. For instance, cobalt-oxygen bonds in $(AE)_xCoP_2O_7$ compounds become more covalent the more ionic the alkaline earth (AE)-oxygen bonds [34]. By analogy, in our $(AE)_{1-x}Co_xTi_2O_5$ solid solutions (with AE = Mg^{2+} ions being replaced by Zn^{2+}), the ionic character of Zn-O bonds is much lower with respect to Mg-O bonds, since the Pauling's electronegativity of Zn (1.6) is considerably higher than that of Mg (1.2). Therefore, and due to

the *competitive bond effect*, replacement of Mg^{2+} by Zn^{2+} in our compositions is expected to reduce the covalence (or increase the ionicity) of competing Co-O bonds in octahedral sites, thus also modifying the crystal field applied on Co^{2+} chromophore ions and the observed color.

3.6. Technological performance of (Co,Zn)-karrooite powders as ceramic pigments or dyes

Finally, the potential application of these greenish (Co,Zn)-karrooite solid solutions as ceramic pigments or dyes for the coloration of low-temperature ceramic glazes was also tested. In order to evaluate their stability and coloring performance, fired pigments were enameled (5 wt% of pigment) within three conventional transparent ceramic glazes (A, B and C) of relatively low firing temperature compressed between 980 and 1050 ºC (the composition details and firing schedules were given in section 2.2). The main research interests were to ascertain whether these Co-doped karrooite pigments were or not sensitive to ceramic glazes rich in alkalis (CaO and ZnO) [2], and also to analyze the effect of Zn-codoping on the stability of these Co-karrooite pigments. Indeed, Zn-containing pigments have been found in some cases to be more stable against chromophore (Co^{2+}) dissolution in the glaze in these more aggressive environments of Zn-Ca-borosilicate melts [35].

The color aspect of glazed samples including the measured color parameters (*L*a*b**) may be seen in Figure 10 for the three pigment series (*Kar-Co*, *Kar-CoZnL* and *Kar-CoZnH*). A very simple and direct indication of the higher or lower stability of these (Co,Zn)-karrooite pigments may be inferred just by visually observing the color change produced or not after enamel firing (980-1050 ºC) in glazed samples. As it may be observed, glazed samples presented rather bluish or turquoise (greenish blue) colorations instead of the original greenish color of pigment powders, and this color change indicates that the pigments did not withstand the chemical attack within the ceramic glazes. Surprisingly, the greenish hue (negative *a** parameter), which can be unambiguously associated to the color of stabilized (not dissolved) Co-karrooite pigment particles, was better preserved in Ca- and Zn-rich ceramic glaze (B) fired at 1050 ºC. In contrast, pigments enameled in glazes with a low Ca and Zn content (A and C) and fired at a lower temperature (980 ºC) presented more turquoise or bluish colorations (negative *b**

parameter), especially in glaze A (free of Pb). This fact is indicative of much lower pigment stability in these glazes. Indeed, this bluish coloration is well-known in the literature to be associated to Co^{2+} ions dissolved and incorporated mainly in tetrahedral environments of the glassy phase, the commonly named "cobalt leaching" or "cobalt bleeding" [4,6,9,10,35,40–43]. In our compositions, the bluish hue of glazed samples was observed to increase with the nominal Co-content in the pigment, which would be therefore indicating a higher incorporation of Co^{2+} within the glassy matrix.

Also noteworthy, codoping with Zn^{2+} ions even at higher levels (*Kar-CoZnH* samples) was not observed to ameliorate significantly the stability of Co-karrooite pigments, which would be followed by a better preservation of the original green color of the pigments. Effectively, it is evident that glazed samples with *Kar-CoZnH* pigments exhibited rather similar turquoise (glaze B) or bluish (glaze C) colorations; however, it must be highlighted that in glaze C the bluish coloration was considerably reduced (having even a yellowish hue with positive b^* value for $x \leq 0.1$) with respect to Zn-free samples.

A complementary, more rigorous and precise confirmation of the relatively low stability of (Co,Zn)-karrooite pigments within the employed ceramic glazes (A, B and C) was also obtained by optical spectroscopy. The Kubelka-Munk (*K/S*) absorbance spectra corresponding to glazed samples with 1200ºC-fired pigments (*Kar-Co*, and *Kar-CoZnH* samples with a constant 20 mol% of Co-doping, $x = 0.2$) are shown in Figure 11. The spectra of the corresponding fired powders have been also included for comparison purposes. As an important remark, the obtained optical spectra of glazed samples may be interpreted as a the sum (convolution) of absorption bands arising from optical transitions associated to octahedral Co^{2+} ions in karrooite pigment particles (remaining still undissolved in the ceramic glaze and imparting a greenish coloration) and those associated to tetrahedral Co^{2+} ions dissolved and incorporated within the glaze (responsible for the bluish color).

Accordingly, the presence of stable karrooite particles dispersed in ceramic glazes may be followed in the spectra by the presence of the sharper, narrower and more intense absorption

band around 550-620 nm (centered at 590 nm) associated to ν_3 transition of octahedral Co^{2+} (named as ν_3^O in Figure 11), and specially by the presence of the characteristic double band in the near-IR region (1100-1600 nm), with the two peaks centered at around 1190 and 1430 nm, unambiguously attributed to ν_1 transition of octahedral Co^{2+} (ν_1^O). Similarly, the presence of Co^{2+} ions incorporated within tetrahedral environments of the glassy phase may be confirmed by the presence of the typical bands associated to tetrahedral Co^{2+}: first of all, the characteristic broad and multiple band spanning the visible region from about 470 to almost 700 nm (with the three peaks being centered at 540, 590, and 640 nm), which arises from ν_3 transition ($^4A_2$ (^4F) $\rightarrow$ $^4T_1$ (^4P)) of tetrahedral Co^{2+} (ν_3^T). This broad band therefore overlaps completely the narrower ν_3^O transition of octahedral Co^{2+}. The three-fold splitting of ν_3^T transition has been attributed to Jahn-Teller distortion of tetrahedral sites [44] and mainly to spin-orbit (L-S Russell-Saunders) coupling effects [43,45]. Then, the remaining ν_2^T and ν_1^T transitions of tetrahedral Co^{2+} ions (to $^4T_1$ (^4F) and $^4T_2$ (^4F) excited terms, respectively) should appear as two broad and less intense bands extending in the near (around 1400 nm) and mid IR range (1600 nm) of the spectrum.

As it may be clearly observed in Figure 11 (above), the optical spectrum of Zn-free *Kar-Co* sample (x = 0.2, $Mg_{0.8}Co_{0.2}Ti_2O_5$) once enameled within glaze B (Ca- and Zn-rich) still clearly retains the absorption bands of octahedral Co^{2+} ions, although the spectrum is rather dominated by the absorption features of tetrahedral Co^{2+} (which are usually more intense due to the relaxation of the Laporte selection rule). In contrast, the optical spectra of *Kar-Co* composition in glazes A and C are much more dominated by the optical absorption features of tetrahedral Co^{2+} ions (especially in glaze A, in agreement with the more bluish color of compositions enameled within this ceramic glaze).

A similar behavior was found in the optical spectra of Zn-rich *Kar-CoZnH* sample (with x = 0.2, $Mg_{0.4}Zn_{0.4}Co_{0.2}Ti_2O_5$) in glazes B and C (Figure 11 below). Again, the typical absorption features of octahedral Co^{2+} coming from karrooite pigment particles were more clearly preserved in glaze B (Ca- and Zn-rich), while in glaze C the absorbance spectrum was mostly

dominated by the transition bands of tetrahedral Co^{2+} ions incorporated in the glaze. Therefore, as it was previously stated, codoping with high amounts of Zn^{2+} ions did not improve the stability of Co-karrooite pigments.

In summary, (Co,Zn)-karrooite green pigments proved to be more stable within the Ca- and Zn-enriched ceramic glaze (B) employed in this this study, and this result is in apparent contradiction with results obtained in previous investigations on the stability of Co-karrooite pigments [2]. Nevertheless, it must be highlighted that the complex oxide-based compositions of the ceramic glazes employed herein and in the previous investigations were not exactly the same.

4. Conclusions

In this study, the synthesis by conventional ceramic route of Co doped ($Mg_{1-x}Co_xTi_2O_5$), Zn doped ($Mg_{1-x}Zn_xTi_2O_5$) and Co- and Zn-codoped karrooite solid solutions ($Mg_{0.8-x}Zn_{0.2}Co_xTi_2O_5$ and $(Mg_{0.5}Zn_{05})_{1-x}Co_xTi_2O_5$) was investigated.

Regarding to reactivity, XRD characterization revealed for the first time the high solid solubility limit of Zn^{2+} in $MgTi_2O_5$ karrooite (between 60 and 80 mol%) at both 1200 or 1400 ºC. In contrast, the addition of Co^{2+} decreased significantly the reactivity and karrooite stabilization in *Kar-Co* ($Mg_{1-x}Co_xTi_2O_5$; without Zn codoping) and *Kar-CoZnL* series ($Mg_{0.8-x}Zn_{0.2}Co_xTi_2O_5$; 20 mol% of Zn). In both cases residual $MgTiO_3$ ilmenite coexisted with karrooite main phase for Co^{2+} doping equal to or above 10 mol%. Very noteworthy, codoping with higher levels of Zn^{2+} (*Kar-CoZnH* compositions, $(Mg_{0.5}Zn_{0.5})_{1-x}Co_xTi_2O_5$; 40-47.5 mol% of Zn) proved to be very effective in the incorporation of Co^{+2} and stabilization of $(Mg,Zn,Co)Ti_2O_5$ pseudobrookite as single crystalline phase.

On the other hand, replacement of Mg^{2+} by the larger Zn^{2+} or Co^{2+} ions in all the composition series was reflected in an anisotropic variation of cell parameters of karrooite lattice, with a general increase of cell volume. However, the microstructure and morphology of

the grain-like aggregates forming the fired powders was not substantially affected by Co^{+2} and Zn^{+2} doping.

Interestingly, the obtained (Co,Zn)-doped karrooite pigments exhibited a gamut of yellowish green colors, which became less yellowish (lower *b** values) and more saturated or darker (lower *L**) the higher the Co content. By *UV–vis–NIR* spectroscopy, the yellowish-green colors were associated with electronic transitions of Co^{2+} located in the two non-equivalent M1 and M2 octahedral sites of karrooite pseudobrookite. Remarkably, codoping with Zn^{2+} ions did not modify significantly the greenish component (similar *-a** values) but diminished substantially the yellow hue (*b**), and resulted also in lighter colors (higher *L**). This color change was caused by the modification of crystal field exerted on Co^{2+} ions and the lower covalence of Co-O bonds induced by Zn^{2+} codoping. This was reflected in the optical spectra by a decreased absorption intensity (optical absorption density) associated with ν_3 ($^4T_{1g}$ (^4F) $\rightarrow$ $^4T_{1g}$ (^4P)) and also to Co-O charge transfer transitions.

Finally, (Co,Zn)-karrooite green pigments behaved rather as ceramic dyes, since glazed samples exhibited turquoise or blue colors associated with Co^{2+} ions dissolved in tetrahedral environments of the glassy phase (the higher the Co content, the bluer the colors). Contrarily to previous reports, these pigments were more stable in a Ca- and Zn-enriched ceramic glaze (B) fired at a higher temperature (1050 ºC). This was evidenced by a better preservation of the green hue and optical absorption features of octahedral Co^{2+} in glazed samples.

Acknowledgements

The authors acknowledge the financial support by "Universitat Jaume I de Castellón" (Project P1.1B2015-19) and by the Spanish "Ministerio de Economía y Competividad" (Project MAT2015-69443-P).

Appendix A. Supplementary data

Supplementary data associated with this article can be found, in the online version, at doi:10.1016/j.ceramint. 20XX.XX.XXX.

References

[1] O. von Knorring, K.G. Cox, Kennedyite, a new mineral of the pseudobrookite series, Mineral. Mag. 32 (1961) 676–682. doi:10.1180/minmag.1961.032.252.02.

[2] F. Matteucci, G. Cruciani, M. Dondi, G. Gasparotto, D.M. Tobaldi, Crystal structure, optical properties and colouring performance of karrooite $MgTi_2O_5$ ceramic pigments, J. Solid State Chem. 180 (2007) 3196–3210. doi:10.1016/j.jssc.2007.08.029.

[3] M. Llusar, E. García, M.T. García, C. Gargori, J.A. Badenes, G. Monrós, Synthesis, stability and coloring properties of yellow–orange pigments based on Ni-doped karrooite $(Ni,Mg)Ti_2O_5$, J. Eur. Ceram. Soc. 35 (2015) 357–376. doi:10.1016/j.jeurceramsoc.2014.08.010.

[4] L. Mantovani, M. Tribaudino, M. Dondi, C. Zanelli, Synthesis and color performance of $CaCoSi_2O_6$ pyroxene, a new ceramic colorant, Dye. Pigment. 120 (2015) 118–125. doi:10.1016/j.dyepig.2015.04.001.

[5] S. Minami, T.; Ghosh, Combustion Syntheses of cobalt pigments: Blue and Pink, Curr. Sci. 78 (2000) 892–896.

[6] M. Dondi, M. Ardit, G. Cruciani, C. Zanelli, Tetrahedrally coordinated Co^{2+} in oxides and silicates: Effect of local environment on optical properties, Am. Mineral. 99 (2014) 1736–1745. doi:10.2138/am.2014.4877.

[7] CPMA, Classification and chemical descriptions of the complex inorganic color pigments, Fourth Edition, (2010) 1–103. www.cpma.com.

[8] J. Zou, W. Zheng, TiO_2@$CoTiO_3$ complex green pigments with low cobalt content and tunable color properties, Ceram. Int. 42 (2016) 8198–8205. doi:10.1016/j.ceramint.2016.02.029.

[9] E. Ozel, H. Yurdakul, S. Turan, M. Ardit, G. Cruciani, M. Dondi, Co-doped willemite ceramic pigments: Technological behaviour, crystal structure and optical properties, J. Eur. Ceram. Soc. 30 (2010) 3319–3329. doi:10.1016/j.jeurceramsoc.2010.08.013.

[10] M. Llusar, A. Forés, J.A. Badenes, J. Calbo, M.A. Tena, G. Monrós, Colour analysis of some cobalt-based blue pigments, J. Eur. Ceram. Soc. 21 (2001) 1121–1130.

doi:10.1016/S0955-2219(00)00295-8.

[11] A. Forés, M. Llusar, J.A. Badenes, J. Calbo, M.A. Tena, G. Monrós, Cobalt minimisation in willemite ($Co_xZn_{2-x}SiO_4$) ceramic pigments, Green Chem. 2 (2000) 93–100. doi:10.1039/b000748j.

[12] M.S. Ghiorso, H. Yang, R.M. Hazen, Thermodynamics of cation ordering in karrooite ($MgTi_2O_5$), Am. Mineral. 84 (1999) 1370–1374. doi:10.2138/am-1999-0914.

[13] A. Navrotsky, Thermodynamics of Formation of Some Compounds with the pseudobrookite structure and of the $FeTi_2O_5$-Ti_3O_5 Solid Solution Series, Am. Mineral. 60 (1975) 249–256.

[14] D.J. Xirouchakis, D.; Smirnov, A.; Woody, K.; Lindsey, D.H.; Andersen, Thermodynamics and stability of pseudobrookite-type $MgTi_2O_5$ (karrooite), Am. Mineral. 87 (2002) 658–667. doi:0003-004X/02/0506–658$05.00.

[15] H. Müller-Buschbaum, M. Waburg, Pseudobrookite mit weitgehend geordneter Metallverteilung: $CoTi_2O_5$, $MgTi_2O_5$ und $FeTi_2O_5$, Monatshefte Für Chemie Chem. Mon. 114 (1983) 21–25. doi:10.1007/BF00809371.

[16] K.T. Jacob, G. Rajitha, Role of entropy in the stability of cobalt titanates, J. Chem. Thermodyn. 42 (2010) 879–885. doi:10.1016/j.jct.2010.02.016.

[17] A. Yankin, O. Vikhreva, V. Balakirev, P–T–x diagram of the Co–Ti–O system, J. Phys. Chem. Solids. 60 (1999) 139–143. doi:10.1016/S0022-3697(98)00058-4.

[18] R.D. Shannon, Revised effective ionic radii and systematic studies of interatomic distances in halides and chalcogenides, Acta Crystallogr. Sect. A. 32 (1976) 751–767. doi:10.1107/S0567739476001551.

[19] M. Dondi, R.A. Eppler, Ceramic Colorants, in: Ullmann's Encycl. Ind. Chem., Wiley-VCH Verlag GmbH & Co. KGaA, Weinheim, Germany, 2014: pp. 1–18. doi:10.1002/14356007.a05_545.pub2.

[20] R.A. Eppler, Colorants for Ceramics, in: Kirk-Othmer Encycl. Chem. Technol., John Wiley & Sons, Inc., Hoboken, NJ, USA, 2002. doi:10.1002/0471238961.0315121505161612.a01.pub2.

[21] G. Monros, Pigment, Ceramic, in: Encycl. Color Sci. Technol., Springer New York, New York, NY, 2013: pp. 1–15. doi:10.1007/978-3-642-27851-8_181-3.

[22] R.A. Eppler, D.R. Eppler, The relative stability of ceramic pigments, Ceram. Eng. Sci. Proc. 18 (1997) 139–149.

[23] E. Ozel, S. Turan, Production and characterisation of iron - chromium pigments and their interactions with transparent glazes, (n.d.). doi:10.1016/S0955-2219(03)00036-0.

[24] H.J. Cha, D.H. Kang, Y.S. Cho, Optimized microwave dielectric properties of Co- and Ca-substituted $Mg_{0.6}Zn_{0.4}TiO_3$, Mater. Res. Bull. 42 (2007) 265–273. doi:10.1016/j.materresbull.2006.06.002.

[25] J.-J. Wang, Study of $(1-x)(Mg_{0.6}Zn_{0.4})_{0.95}Co_{0.05}TiO_3–xCa_{0.61}Nd_{0.26}TiO_3$ microwave dielectrics, J. Alloys Compd. 486 (2009) 423–426. doi:10.1016/j.jallcom.2009.06.184.

[26] Y.H. Kim, Hyo Tae; Kim, High frequency dielectric ceramic composition and fabrication method thereof, 5,767,030, 1998.

[27] G.N. Shelovanova, T.N. Patrusheva, A.I. Khol'kin, Preparation of photoactive materials based on porous silicon, Theor. Found. Chem. Eng. 43 (2009) 719–722. doi:10.1134/S0040579509050170.

[28] F.H. Dulin, D.E. Rase, Phase Equilibria in the System ZnO-TiO_2, J. Am. Ceram. Soc. 43 (1960) 125–131. doi:10.1111/j.1151-2916.1960.tb14326.x.

[29] S.F. Bartram, R.A. Slepetys, Compound Formation and Crystal Structure in the System ZnO-TiO_2, J. Am. Ceram. Soc. 44 (1961) 493–499. doi:10.1111/j.1151-2916.1961.tb13712.x.

[30] U. Steinike, B. Wallis, Formation and Structure of Ti-Zn-Oxides, Cryst. Res. Technol. 32 (1997) 187–193. doi:10.1002/crat.2170320119.

[31] Y.-C. Liang, C.-Y. Hu, Y.-C. Liang, Crystallographic phase evolution of ternary Zn–Ti–O nanomaterials during high-temperature annealing of ZnO–TiO_2 nanocomposites, CrystEngComm. 14 (2012) 5579. doi:10.1039/c2ce25347j.

[32] N.H. Perry, V. Stevanovic, L.Y. Lim, T.O. Mason, Discovery of a ternary pseudobrookite phase in the earth-abundant Ti–Zn–O system, Dalt. Trans. 45 (2016) 1572–1581. doi:10.1039/C5DT04145G.

[33] R.G. Burns, Mineralogical Applications of Crystal Field Theory, Cambridge University Press, Cambridge, 1993. doi:10.1017/CBO9780511524899.

[34] A. El Jazouli, B. Tbib, A. Demourgues, M. Gaudon, Structure and colour of diphosphate pigments with square pyramid environment around chromophore ions (Co^{2+}, Ni^{2+}, Cu^{2+}), Dye. Pigment. 104 (2014) 67–74. doi:10.1016/j.dyepig.2013.11.021.

[35] M. Dondi, C. Zanelli, M. Ardit, G. Cruciani, Co-Doped Hardystonite, $Ca_2(Zn,Co)Si_2O_7$, a New Blue Ceramic Pigment, J. Am. Ceram. Soc. 94 (2011) 1025–1030. doi:10.1111/j.1551-2916.2010.04203.x.

[36] CIE, Recommendations on Uniform Color Spaces, Color-difference Equations, Psychometric Color Terms, in: Suppl. N° 2 CIE PUbl. N° 15 1971, Bureau Central de la CIE, Paris, 1978.

[37] B.A. Wechsler, A. Navrotsky, Thermodynamics and structural chemistry of compounds in the system MgO-TiO_2, J. Solid State Chem. 55 (1984) 165–180. doi:10.1016/0022-4596(84)90262-7.

[38] H. Yang, R.M. Hazen, Crystal Chemistry of Cation Order–Disorder in Pseudobrookite-Type $MgTi_2O_5$, J. Solid State Chem. 138 (1998) 238–244. doi:10.1006/jssc.1998.7775.

[39] A.B.P. Lever, Inorganic electronic spectroscopy, 2nd ed., Elsevier Science Publishers, Amsterdam, 1984.

[40] M. El Hadri, H. Ahamdane, M.A. El Idrissi Raghni, Sol gel synthesis of forsterite, M-doped forsterite (M=Ni, Co) solid solutions and their use as ceramic pigments, J. Eur. Ceram. Soc. 35 (2015) 765–777. doi:10.1016/j.jeurceramsoc.2014.09.024.

[41] M. Gaudon, L.C. Robertson, E. Lataste, M. Duttine, M. Ménétrier, A. Demourgues, Cobalt and nickel aluminate spinels: Blue and cyan pigments, Ceram. Int. 40 (2014) 5201–5207. doi:10.1016/j.ceramint.2013.10.081.

[42] A. Thulasiramudu, S. Buddhudu, Optical characterization of Mn^{2+}, Ni^{2+} and Co^{2+} ions doped zinc lead borate glasses, 102 (2006) 212–227. doi:10.1016/j.jqsrt.2006.02.006.

[43] D. Möncke, M. Papageorgiou, A. Winterstein-Beckmann, N. Zacharias, Roman glasses coloured by dissolved transition metal ions: Redox-reactions, optical spectroscopy and ligand field theory, 46 (2014) 23–36. doi:10.1016/j.jas.2014.03.007.

[44] C.R. Bamford, The application of the ligand field theory to coloured glasses, Phys. Chem. Glas. 3 (1962) 189–202.

[45] T. Bates, Ligand field theory and absorption spectra of transition-metal ions in glasses,

Vol. 2, in: J.D. Mackenzie (Ed.), Mod. Asp. Vitr. State, Butterworths, London, 1961: pp. 195–254.

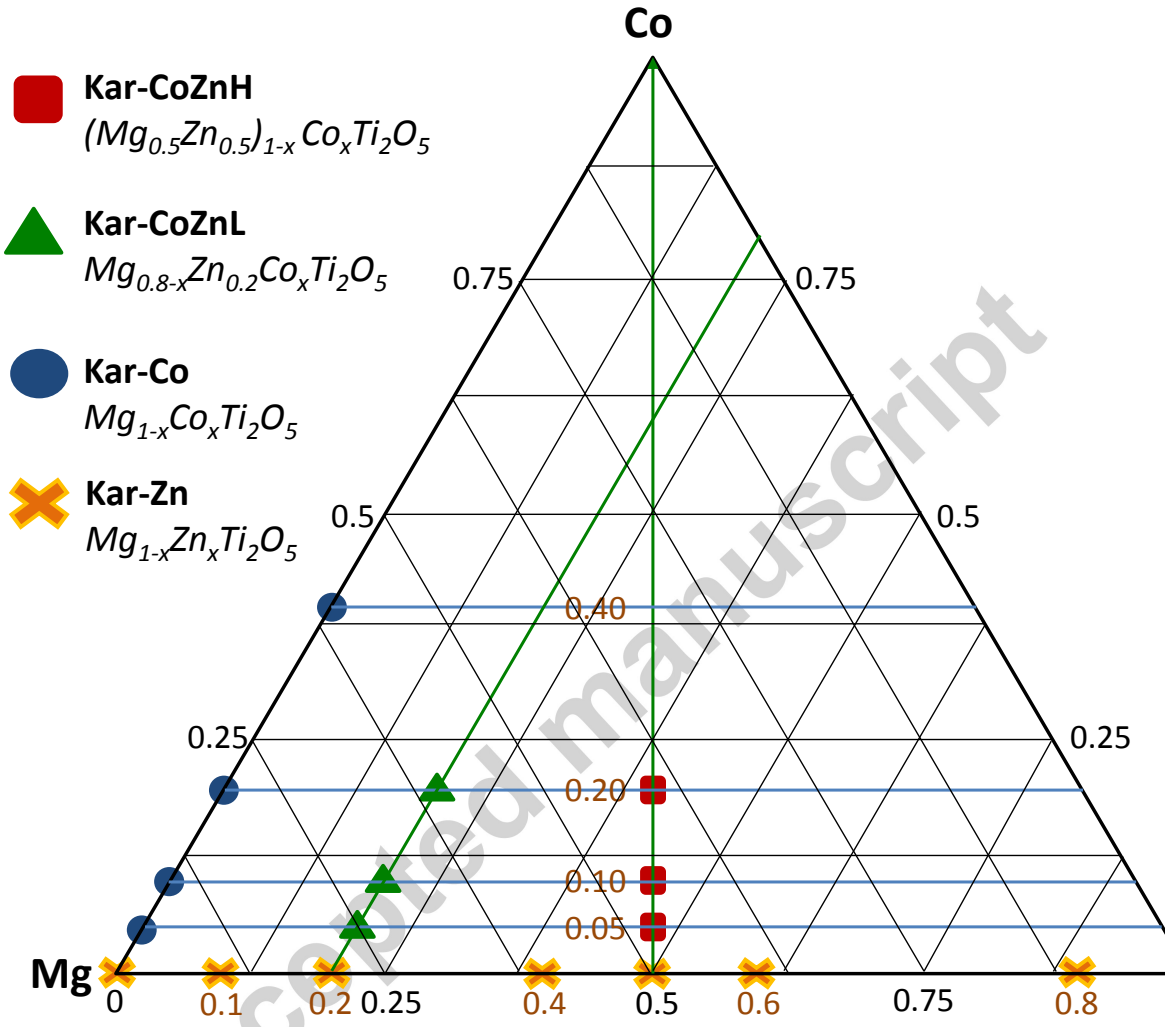

Figure 1. Ternary Mg-Zn-Co diagram showing the location of the prepared compositions for the four *(Co,Zn)-Karrooite* solid solution series: ***a) Kar-Zn***, $Mg_{1-x}Zn_xTi_2O_5$; ***b) Kar-Co***, $Mg_{1-x}Co_xTi_2O_5$; ***c) Kar-CoZnL***, $Mg_{0.8-x}Zn_{0.2}Co_xTi_2O_5$; and ***d) Kar-CoZnH***, $(Mg_{0.5}Zn_{0.5})_{1-x}Co_xTi_2O_5$.

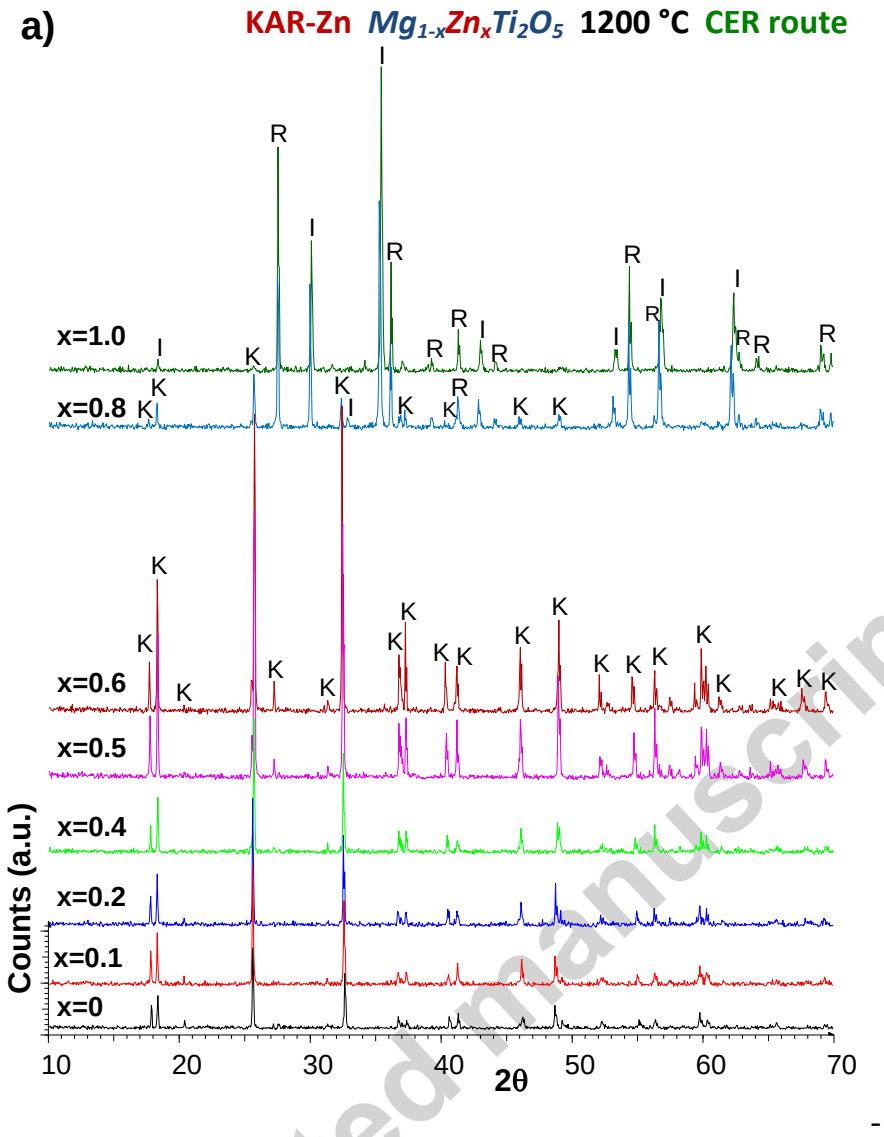

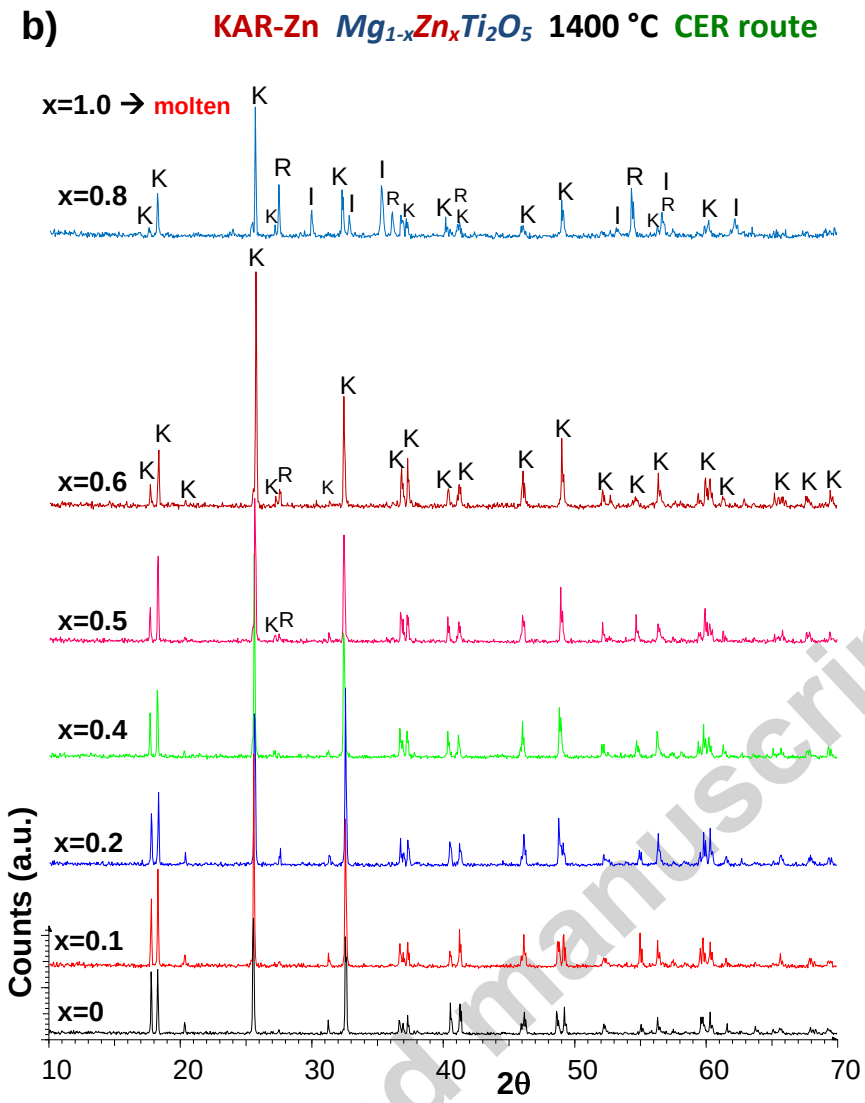

Figure 2. XRD patterns of *Zn-Karrooite* solid solutions (***$Mg_{1-x}Zn_xTi_2O_5$***) prepared by the ceramic route and fired directly at **1200 ºC** for 3h **(a)**, and subsequently at **1400 ºC** for 3h *Crystalline phases:* ***K*** = Pseudobrookite (karrooite) $MgTi_2O_5$ or $(Mg,Zn)Ti_2O_5$ solid solution, ***I*** = Ilmenite (geikielite) $MgTiO_3$ or $(Mg,Zn)TiO_3$ solid solution, and R = Rutile TiO_2 (the composition with x=1.0 melted (vitreous phase) after firing at 1400 ºC/3h and could not be analysed by XRD).

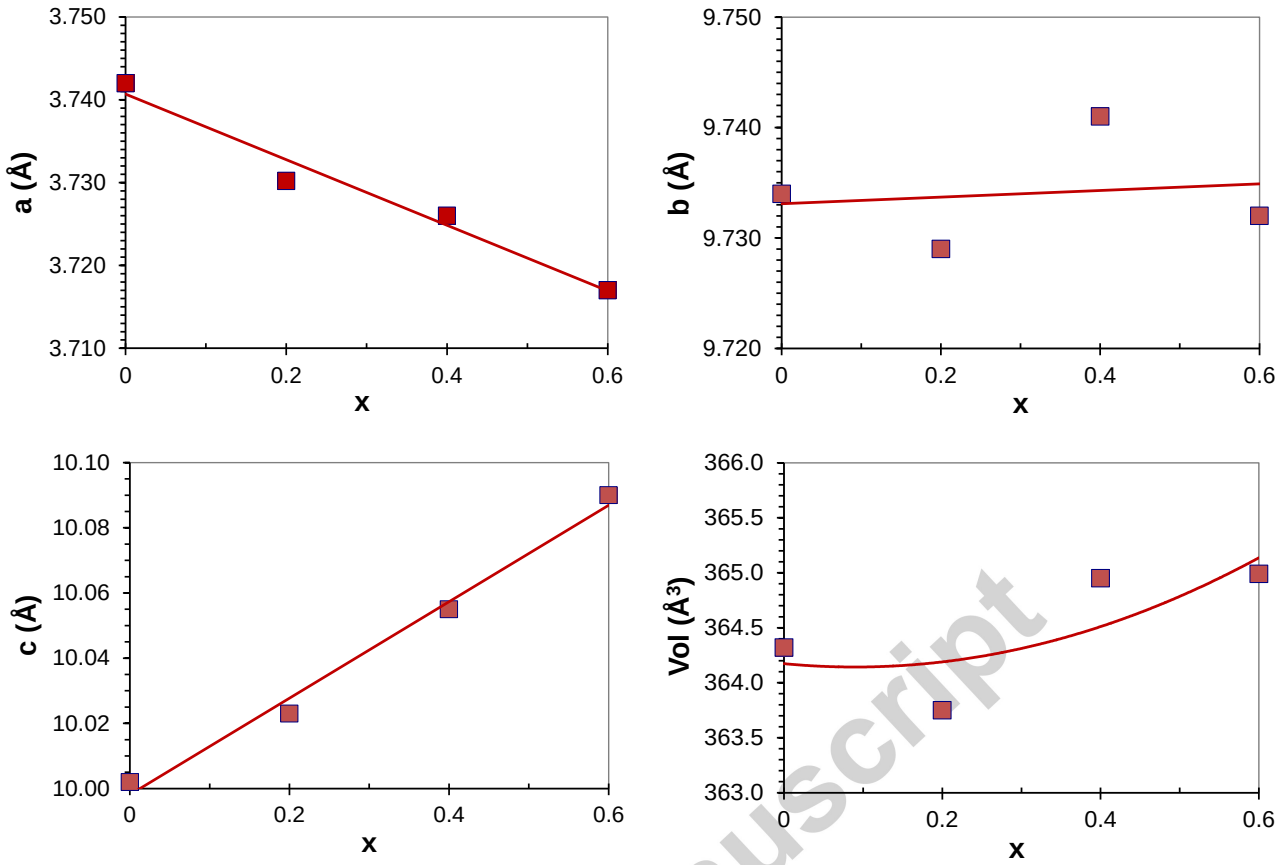

Figure 3. Evolution of cell parameters (*a*, *b* and *c*) and cell volume (*Vol*) with Zn doping (*x*) in ***Kar-Zn*** solid solutions ($Mg_{1-x}Zn_xTi_2O_5$) fired at 1200 °C (3h).

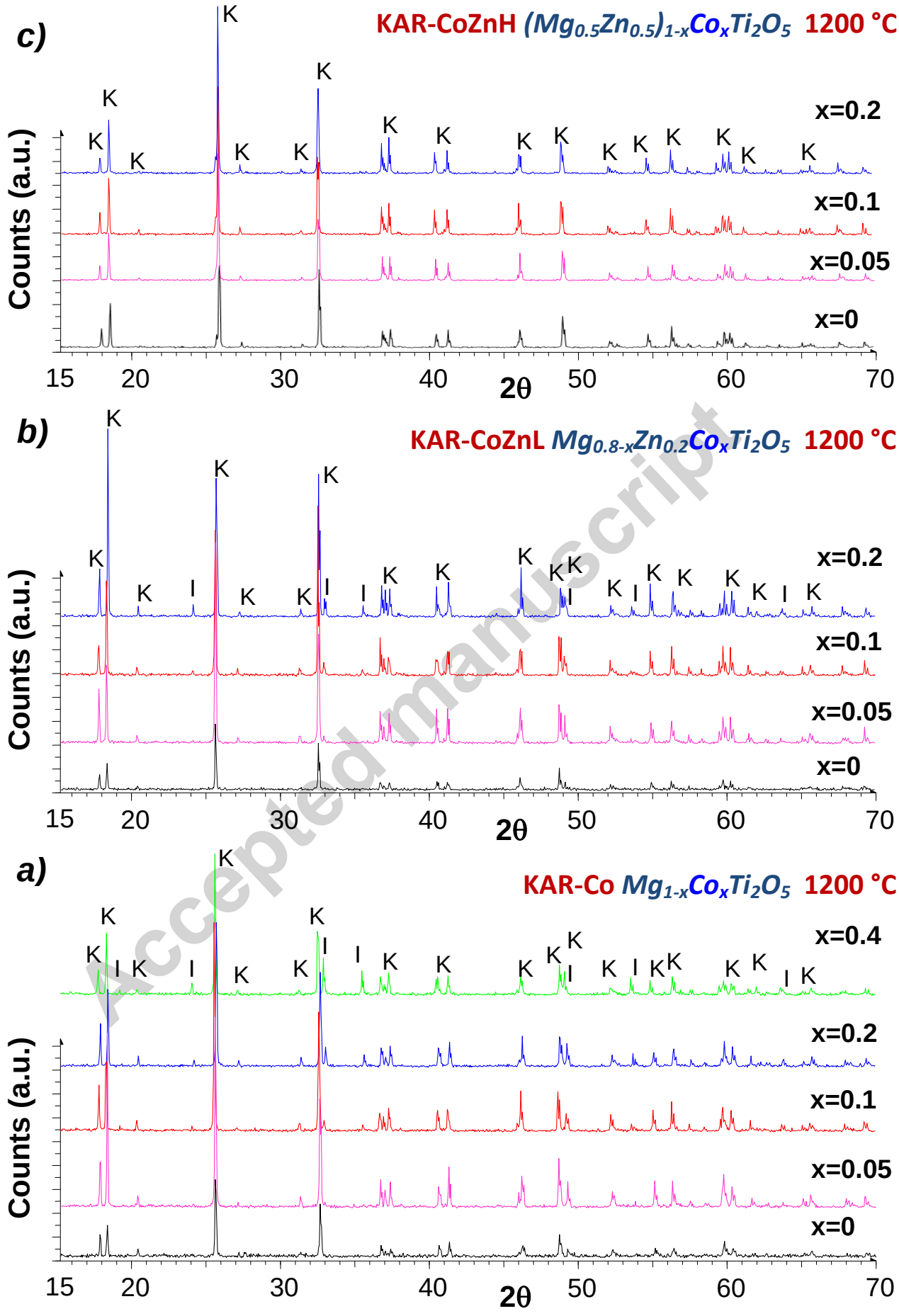

Figure 4. XRD patterns of *(Co,Zn)-Karrooite* solid solution pigments prepared by the ceramic route and fired at **1200 ºC**: ***a) Kar-Co***, $Mg_{1-x}Co_xTi_2O_5$; ***b) Kar-CoZnL***, $Mg_{0.8-x}Zn_{0.2}Co_xTi_2O_5$; ***c) Kar-CoZnH***, $(Mg_{0.5}Zn_{0.5})_{1-x}Co_xTi_2O_5$; *Crystalline phases:* ***K*** = Pseudobrookite (karrooite) $MgTi_2O_5$ or $(Mg,Zn,Co)Ti_2O_5$; ***I*** = Ilmenite (geikielite) $MgTiO_3$ or $(Mg,Zn,Co)TiO_3$.

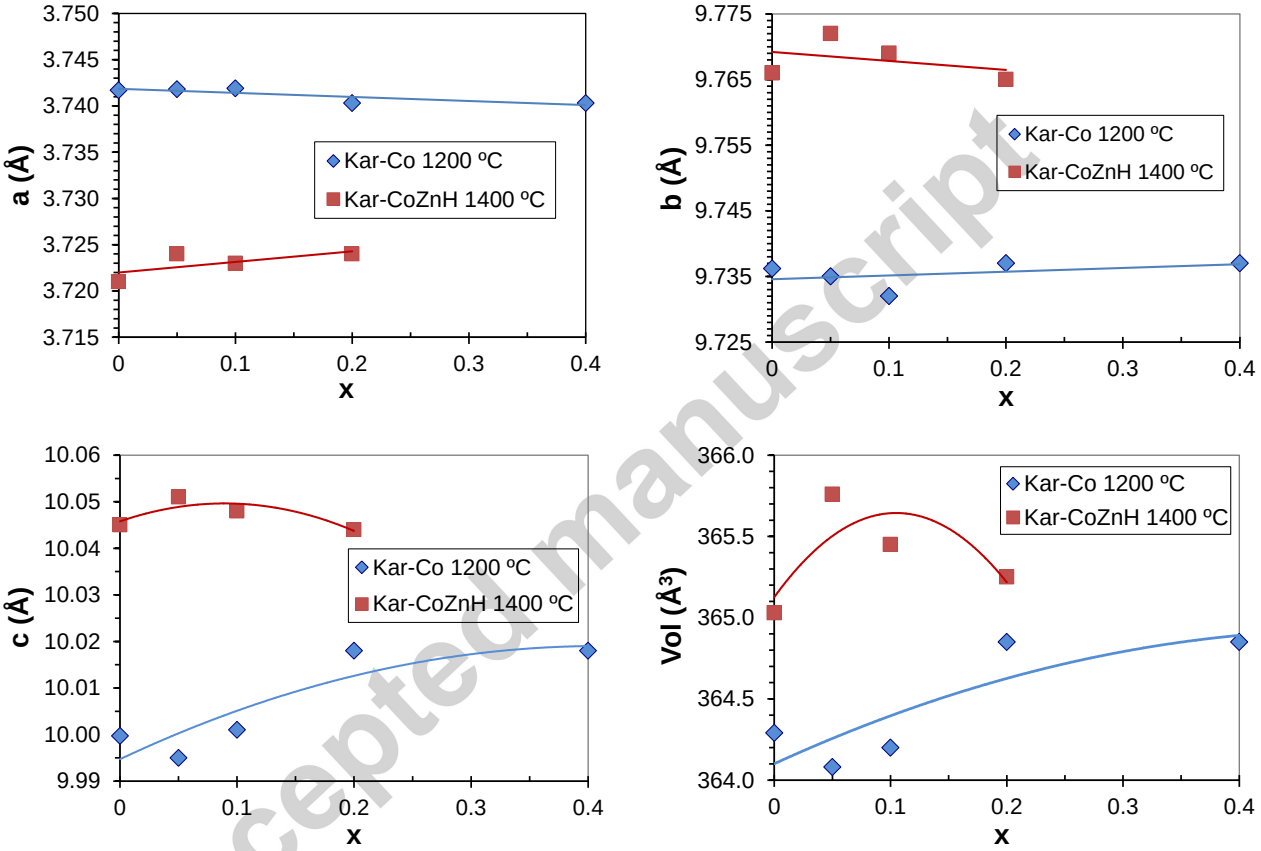

Figure 5. Evolution of cell parameters (*a*, *b* and *c*) and cell volume (*Vol*) with Co doping (*x*) in *Kar-Co* ($Mg_{1-x}Co_xTi_2O_5$) and *Kar-CoZnH* ($(Mg_{0.5}Zn_{0.5})_{1-x}Co_xTi_2O_5$) solid solutions fired at 1200 °C and 1400 °C, respectively.

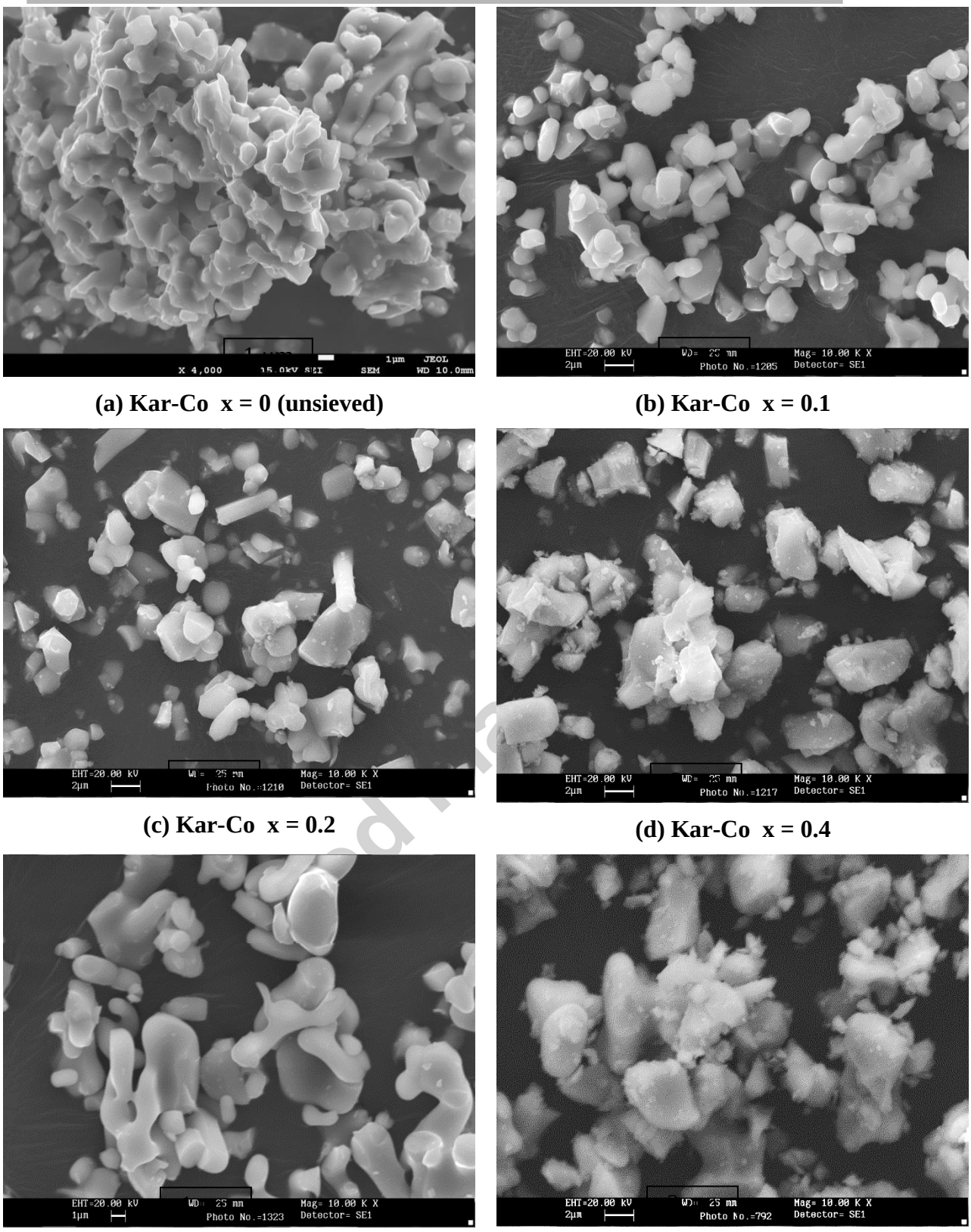

(a) Kar-Co x = 0 (unsieved) **(b) Kar-Co x = 0.1**

(c) Kar-Co x = 0.2 **(d) Kar-Co x = 0.4**

(e) Kar-CoZnL x = 0.2 **(f) Kar-CoZnH x = 0.2**

Figure 6.- SEM images of ***(Co,Zn)-Karrooite*** solid solutions prepared by the ceramic route and fired at 1200 ºC: ***a) to d) Kar-Co***, $Mg_{1-x}Co_xTi_2O_5$ (x = 0, 0.1, 0.2 and 0.4, respectively); ***e) Kar-CoZnL***, $Mg_{0.8-x}Zn_{0.2}Co_xTi_2O_5$ (x = 0.2); and ***c) Kar-CoZnH***,

$(Mg_{0.5}Zn_{0.5})_{1-x}Co_xTi_2O_5$ (x = 0.2). The length of the bar (1 or 2 μm) is indicated in all cases.

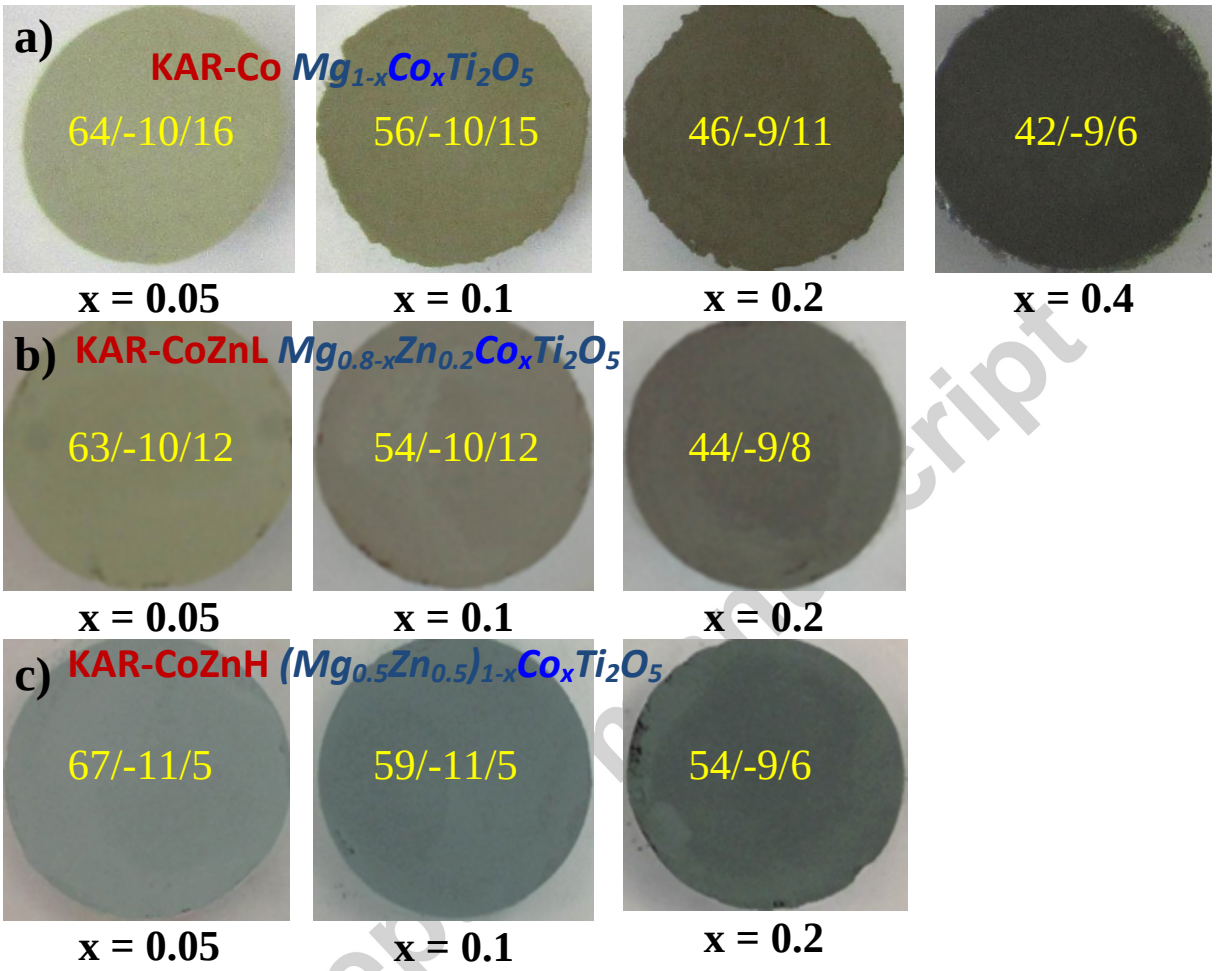

Figure 7. Color aspect of *(Co,Zn)-Karrooite* pigments prepared by the ceramic route and fired directly at **1200 ºC** (3 h soaking): ***a) Kar-Co***, $Mg_{1-x}Co_xTi_2O_5$; ***b) Kar-CoZnL***, $Mg_{0.8-x}Zn_{0.2}Co_xTi_2O_5$; ***c) Kar-CoZnH***, $(Mg_{0.5}Zn_{0.5})_{1-x}Co_xTi_2O_5$; The corresponding color parameters (*L*a*b**) are also indicated (For interpretation of references to color in this Figure the reader is referred to the web version of the article).

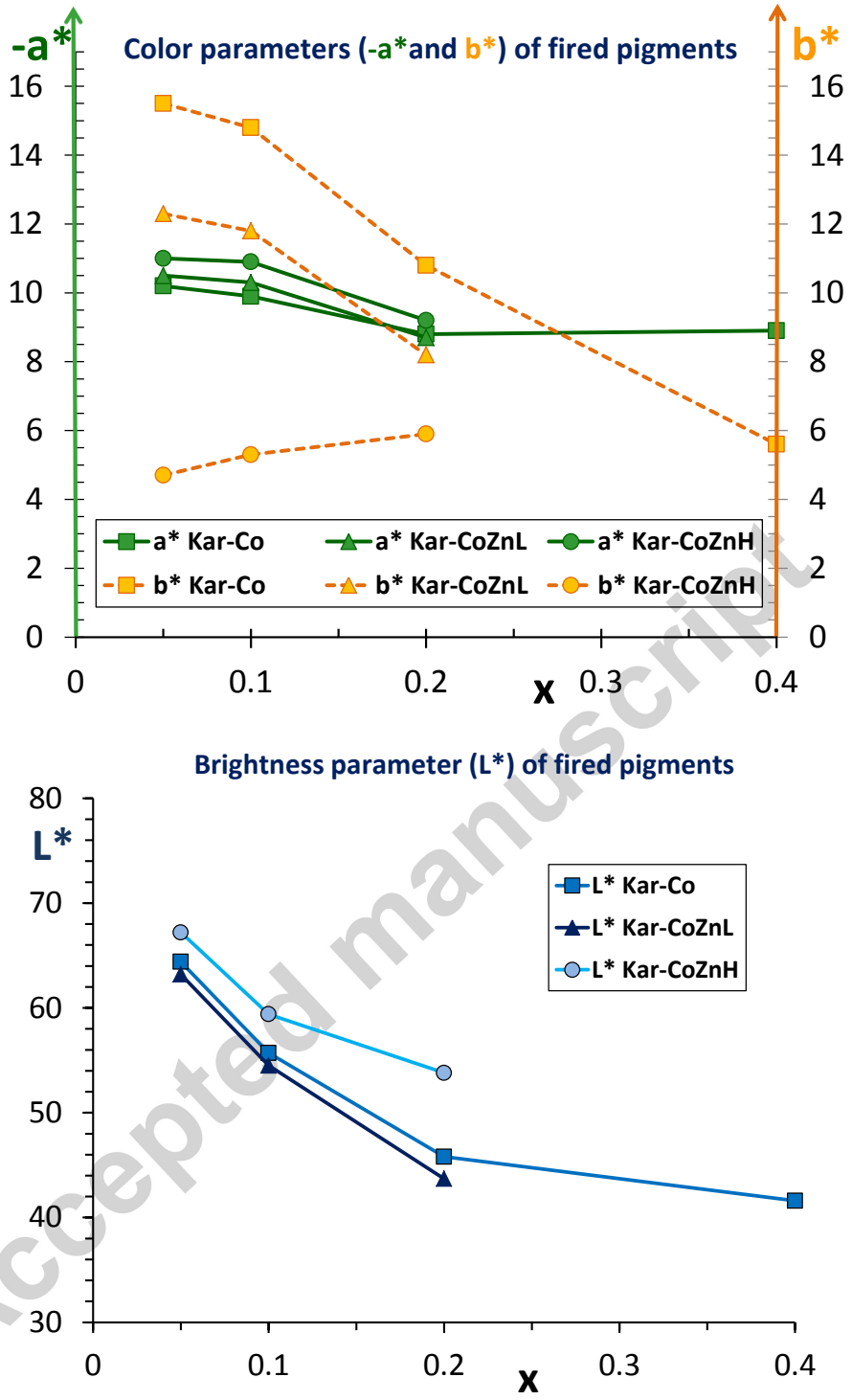

Figure 8. Evolution of color parameters (green hue ***-a****, yellow hue ***+b****, and brightness ***L****) with Co doping (*x*) in ***Kar-Co*** ($Mg_{1-x}Co_xTi_2O_5$), ***Kar-CoZnL*** ($Mg_{0.8-x}Zn_{0.2}Co_xTi_2O_5$) and ***Kar-CoZnH*** $(Mg_{0.5}Zn_{0.5})_{1-x}Co_xTi_2O_5$ solid solutions fired at 1200 °C (3h).

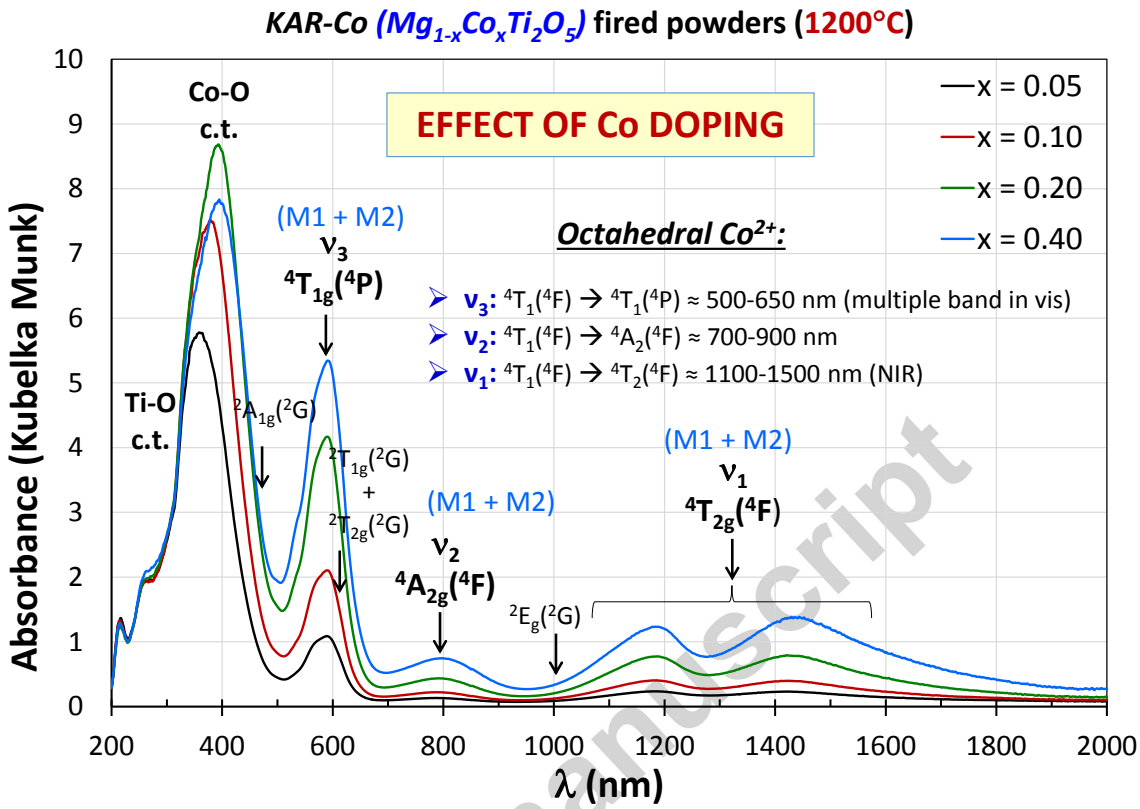

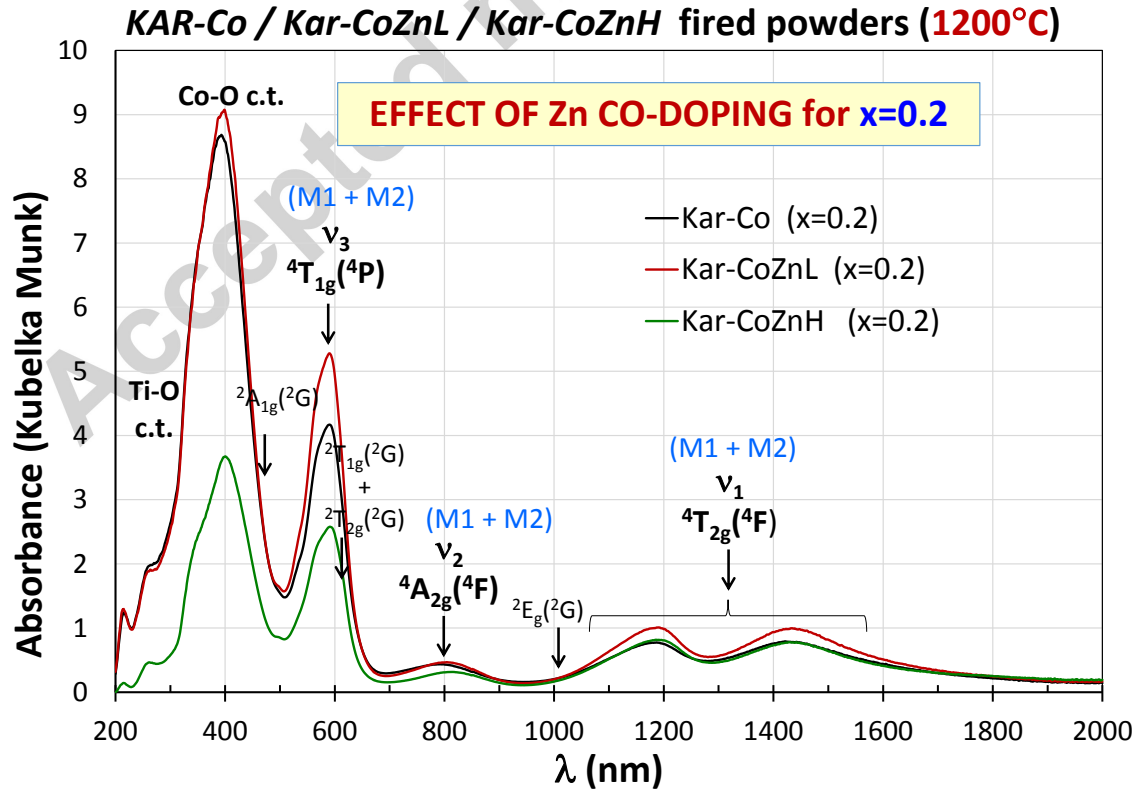

Figure 9.- UV-vis-NIR (Kubelka-Munk) absorption spectra of ***(Co,Zn)-Karrooite*** solid solutions prepared by the ceramic route and fired at 1200 ºC; ***above: Kar-Co***, $Mg_{1-x}Co_xTi_2O_5$ (x = 0.05, 0.1, 0.2 and 0.4). ***below: Kar-Co*** *(x=0.2, $Mg_{0.8}Co_{0.2}Ti_2O_5$)*, ***Kar-CoZnL*** *(x=0.2, $Mg_{0.6}Co_{0.2}Zn_{0.2}Ti_2O_5$)*, and ***Kar-CoZnH*** *(x=0.2, $Mg_{0.4}Co_{0.2}Zn_{0.4}Ti_2O_5$)*.

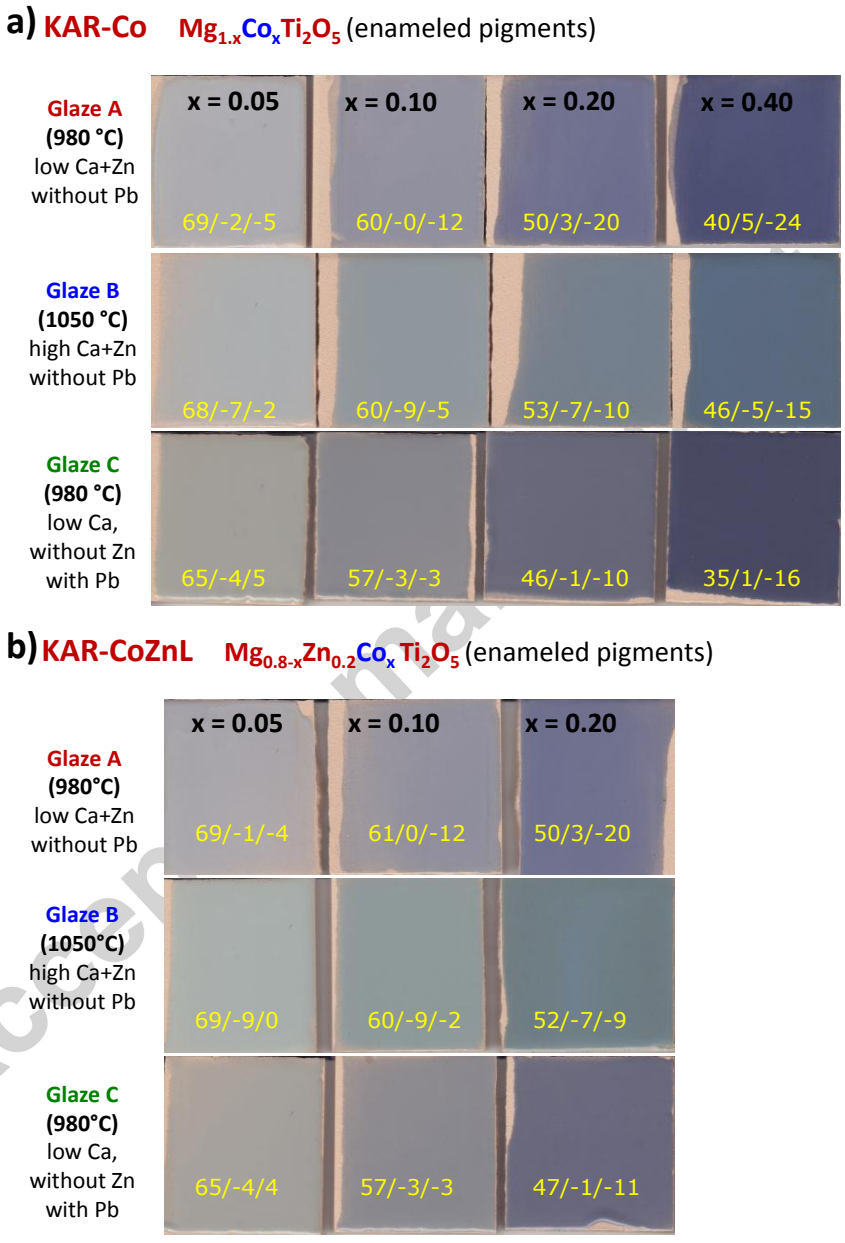

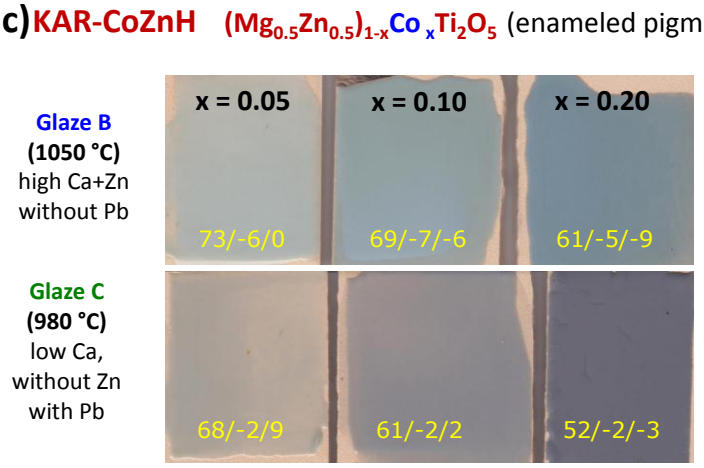

Figure 10. Color aspect of *(Co,Zn)-Karrooite* pigments enameled within different ceramic glazes (A, B and C): ***a) Kar-Co***, $Mg_{1-x}Co_xTi_2O_5$; ***b) Kar-CoZnL***, $Mg_{0.8-x}Zn_{0.2}Co_xTi_2O_5$; ***c) Kar-CoZnH***, $(Mg_{0.5}Zn_{0.5})_{1-x}Co_xTi_2O_5$; The corresponding color parameters (*L*/a*/b**) are also indicated (For interpretation of references to color in this Figure the reader is referred to the web version of the article).

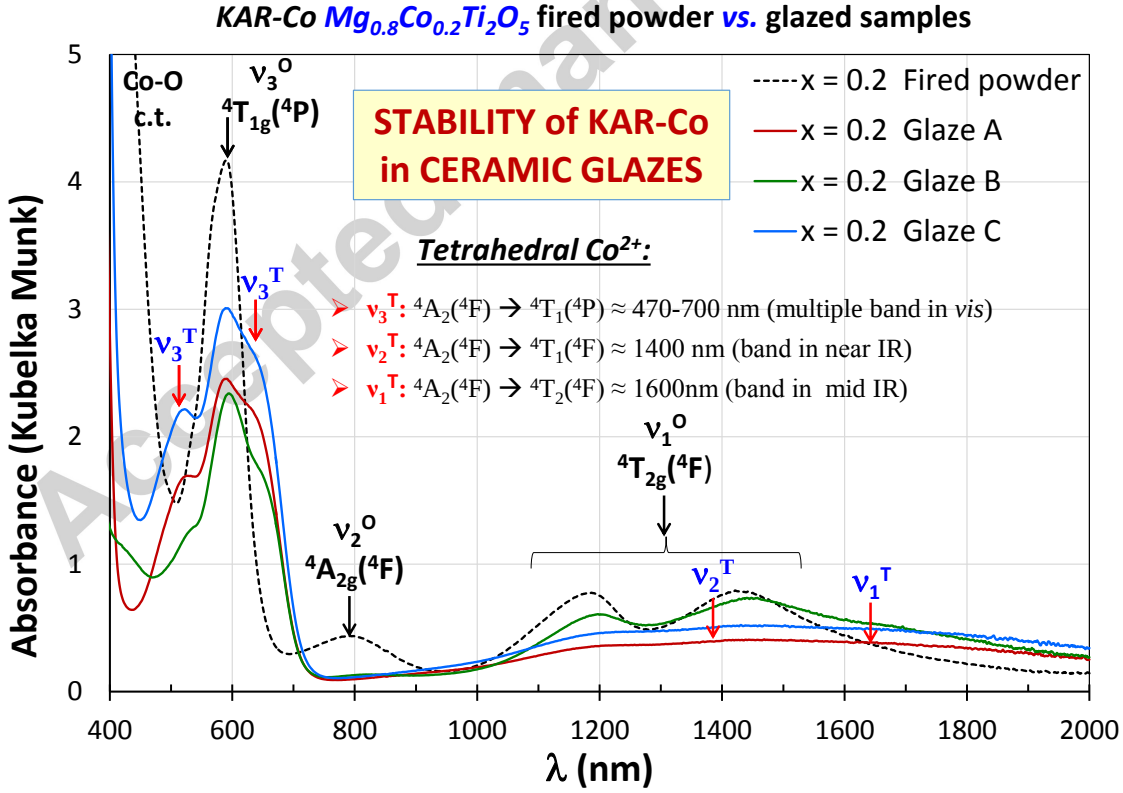

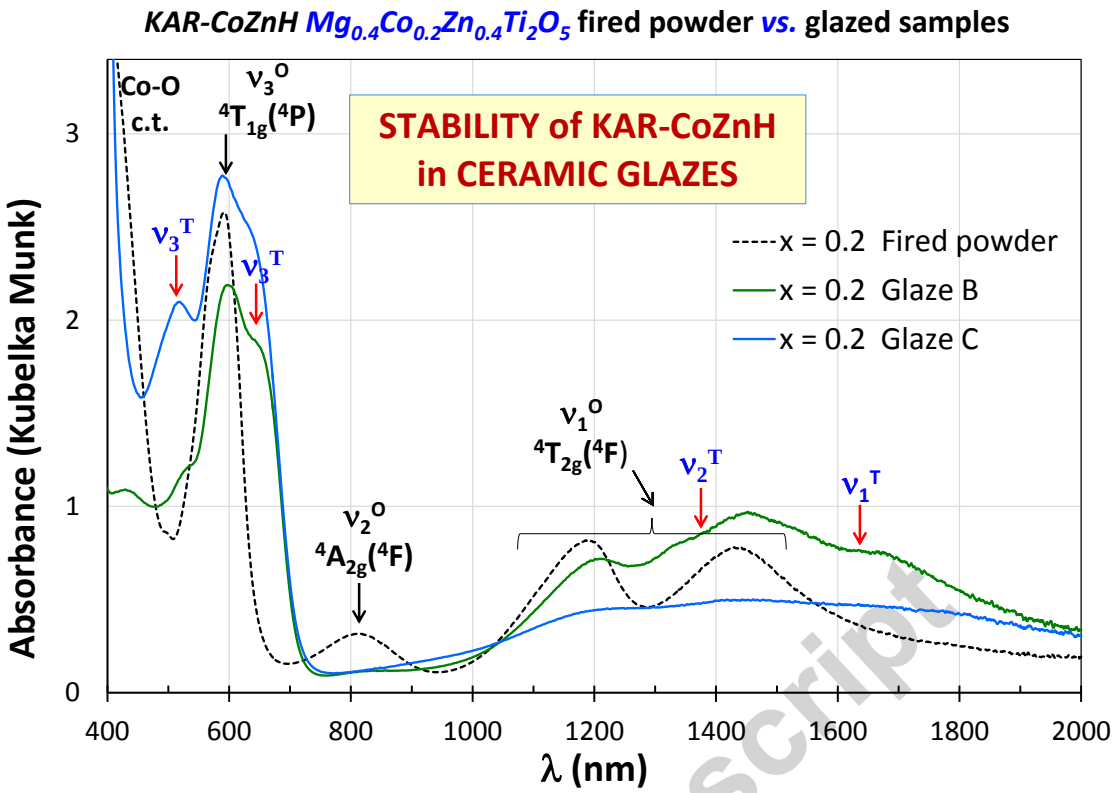

Figure 11.- Comparison of UV-vis-NIR (Kubelka-Munk) absorption spectra of ***Kar-Co*** (x=0.2, $Mg_{0.8}Co_{0.2}Ti_2O_5$, above) and ***Kar-CoZnH*** *(x=0.2, $Mg_{0.4}Co_{0.2}Zn_{0.4}Ti_2O_5$,* below) fired powders (1200 ºC) with the spectra of their corresponding glazed samples within glazes **A** (low CaO and ZnO content, without Pb, fired at 980 ºC), **B** (high CaO and ZnO content, without Pb, fired at 1050 ºC), and **C** (low CaO content, without ZnO, and with a small amount of Pb, fired at 980 ºC).

Table 1. Theoretical (nominal) and experimental samples composition (obtained from average EDX semiquantitative analyses) for *(Co,Zn)-Karrooite* solid solutions fired at 1200 ºC. Standard deviation is given between brackets.

Samples	***Theoretical compositions***	***Average compositions (EDX)***				
		Mg	**Co**	**Zn**	**Ti(*)**	**O**
Kar-Co (x = 0)	$MgTi_2O_5$	1.01 (4)	--	--	2.00	5.01 (4)
Kar-Co (x = 0.1)	$Mg_{0.9}Co_{0.1}Ti_2O_5$	0.86 (2)	0.15 (3)	--	2.00	5.01 (3)

Kar-Co (x = 0.2)	$Mg_{0.8}Co_{0.2}Ti_2O_5$	0.76 (7)	0.31 (5)	--	2.00	5.08 (8)
Kar-Co (x = 0.4)	$Mg_{0.6}Co_{0.4}Ti_2O_5$	0.55 (11)	0.56 (5)	--	2.00	5.11 (16)
Kar-CoZnL (x = 0.1)	$Mg_{0.7}Co_{0.1}Zn_{0.2}Ti_2O_5$	0.66 (6)	0.13 (1)	0.21 (4)	2.00	5.01 (3)
Kar-CoZnL (x = 0.2)	$Mg_{0.6}Co_{0.2}Zn_{0.2}Ti_2O_5$	0.48 (1)	0.22 (7)	0.20 (1)	2.00	4.90 (6)
Kar-CoZnH (x = 0.2)	$Mg_{0.4}Co_{0.2}Zn_{0.4}Ti_2O_5$	0.34 (3)	0.22 (2)	0.43 (3)	2.00	4.90 (6)

(*) The EDX analyses have been normalized to 2 mols of Ti